UNIVERSITÀ DELLA CALABRIA

UNIVERSITA' DELLA CALABRIA

Dipartimento di Fisica

Doctorate School of Science and Technique
"Bernardino Telesio"

A thesis submitted for the degree of Doctor of Philosophy in Science and Technology of Mesophases and Molecular Materials

PON Regione Calabria FSE

Cycle XXVI

02/B1 FIS/03

"ACTIVE PLASMONICS IN SOFT MATTER DOPED WITH GOLD NANOPARTICLES"

"PLASMONICA ATTIVA IN MATERIA SOFFICE DROGATA CON NANOPARTICELLE D'ORO"

School Director
Prof. Roberto Bartolino

Supervisor
Prof. Roberto Caputo

Curriculum Coordinator
Prof. Carlo C Versace

Candidate
Dott. Ugo Cataldi

December 2013

To my family

***"La presente tesi è cofinanziata con il sostegno della Commissione Europea, Fondo Sociale Europeo e della Regione Calabria. L'autore è il solo responsabile di questa tesi e la Commissione Europea e la Regione Calabria declinano ogni responsabilità sull'uso che potrà essere fatto delle informazioni in essa contenute"*.**

Contents

Pubblications

L. De Sio, R. Caputo, U. Cataldi and C.P. Umeton**.,** **Broad Band tuning of the plasmonic resonance of gold nanoparticles hosted in self-organized materials** *J. Mater. Chem***.,** 2011,21, 18967-18970

U. Cataldi, P.Cerminara, L. De Sio, R.Caputo, C.P. Umeton*,* **Fabrication and characterization of strechable PDMS structures doped with Au nanoparticles** Molecul Crystals and Liquid Crystals,558:1,22-27

R. Caputo, L. De Sio, U. Cataldi & C. Umeton (2012) ,**Plasmon Resonance Tunability of Gold Nanoparticles Embedded in a Confined Cholesteric Liquid Crystal Host** Molecular Crystals and Liquid Crystals, 559:1, 194-201

R. Caputo, Ugo Cataldi, A. Cunningham, L. De Sio, T. Bürgi, C. Umeton, **Gold nanoparticles embedded in flexible materials: new frontiers in Plasmonics,** Asia Communications and Photonics Conference 2012/11/7

L. De Sio; R. Caputo; U. Cataldi; J. Dintinger; H. Sellame;T. Scharf; C. Umeton **"Metallic subentities embedded in micro-periodic composite structure (Proceedings Paper)"** Proceeding SPIE, vol. 8114(2011), DOI: 10.1117/12.892777

Roberto Caputo, Luciano De Sio, Ugo Cataldi, Cesare Umeton

Active Plasmonic in Self-Organized Soft Materials

Amorphous Nanophotonics 307-326, 2013/1/1 Springer

Keywords

Active plasmonics, soft matter, metallic nanoparticles, policryps, liquid crystal, cholesteric liquid crystal, PDMS, elastomers, top-down, bottom-up, self-organisation, self-assembling , plasmonics, near-field, electromagnetic coupling , metamaterials, polyelectrolytes, substrate functionalisation, electrostatic assembly, plasmon ruler, dipole potenzial energy, plasmon shift, seeding growing.

Abstract

The main objective of this study is active plasmonics. The work has been focussed on the design, characterization and theoretical interpretation of novel systems. Top-down and bottom-up, self-assembling, approaches have been utilized to realize devices where spherical gold nanoparticles have been periodically and randomly arranged. Two main paths have been followed to achieve this goal.

In the first one, by utilizing a rigid periodic structure as a host platform for soft-matter (cholesteric liquid crystals) mixed with plasmonic nano-entities, was possible to obtain a chirally-organized tuneable plasmonic system. The tunability of the obtained device has been induced by applying temperature changes or external electric fields.

In the second one, the surface of an elastomeric platform has been randomly covered by gold-nanoparticles. Controlled nano-chemistry processes have been successively applied to the nanoparticles (immobilized on the surface) to locally increase their size. The elastic properties of the template together with the increased size of particles have allowed a systematic study of the coupling between near-fields of the spherical nanostructures.

Colloidal nano-chemistry technics have been utilized both to synthetize spherical gold nano-particles and to increase their sizes. Spectroscopic analysis has been used to analyse the response of obtained structures under electrical, thermodynamical and mechanical stimuli.

SEM and TEM imaging have been exploited to study the morphology of devices, the shape of nano-structures and to measure their sizes. Moreover, from SEM images, through the use of a MatLab code written to the purpose, it has been possible to extract fundamental parameters used to perform a theoretical analysis of experimental results.

Riassunto in Italiano.

Il principale obiettivo di questo studio è la Plasmonica Attiva. Il lavoro è stato focalizzato sulla progettazione e la caratterizzazione di nuovi sistemi e la spiegazione teorica degli stessi. Al fine di realizzare queste strutture con nanoparticelle d'oro sferiche, disposte periodicamente e casualmente, sono stati utilizzati procedimenti di auto-assemblaggio in configurazioni top-down e bottom-up.

Per raggiungere questi obiettivi sono state seguite principalmente due strade.

Nella prima si sono prodotti sistemi plasmonici tunabili a organizzazione chirale attraverso l'uso di una piattaforma rigida e periodica con la funzione di ospitare materia soffice, quali cristalli liquidi colesterici, mescolata con nano-unità plasmoniche. La tunabilità di questi dispositivi è stata resa possibile dall'applicazione agli stessi di campi elettrici esterni e attraverso variazioni di temperatura.

Nella seconda, la superficie di una piattaforma elastomerica è stata ricoperta in modo casuale da nanoparticelle d'oro. Le stesse (immobilizzate sulla superficie), sono state trattate, in modo controllato, con processi di nano-chimica al fine di incrementare localmente le loro dimensioni. La sinergia tra le proprietà elastiche del substrato e l'aumento di taglia delle particelle ha permesso lo studio sistematico dell'accoppiamento tra campi vicini delle nanostrutture sferiche.

Al fine di sintetizzare e di accrescere le nanoparticelle sferiche, sono state utilizzate tecniche di nano-chimica colloidale. La risposta ottica di entrambi i tipi di strutture, sotto l'azione elettrica, termodinamica e meccanica, è stata ottenuta tramite analisi spettroscopica.

Inoltre le tecniche SEM e TEM sono state sfruttate per eseguire la caratterizzazione morfologica di entrambi i sistemi e delle loro nanostrutture e per misurarne le dimensioni.

Infine, attraverso l'utilizzo di immagini SEM e tramite codici scritti ad hoc con il programma MatLab, è stato possibile estrarre le misure di alcuni parametri fondamnetali, utilizzati successivamente per eseguire le analisi teoriche sui risultati sperimentali.

Introduction

"There's Plenty of Room at the Bottom", was a famous lecture given by the physicist Richard Feynman in 1959. Nowadays, this paper is universally considered the beginning of Nanotechnology.

In these years, the topic has been extensively explored and new amazing properties of matter have been discovered at the nanoscale. Experimental and theoretical studies of the interaction between electromagnetic fields and metal or semi-conductor nanostructures, particularly nanoparticles, have found noticeable application in several fields, as illustrated in the figure below.

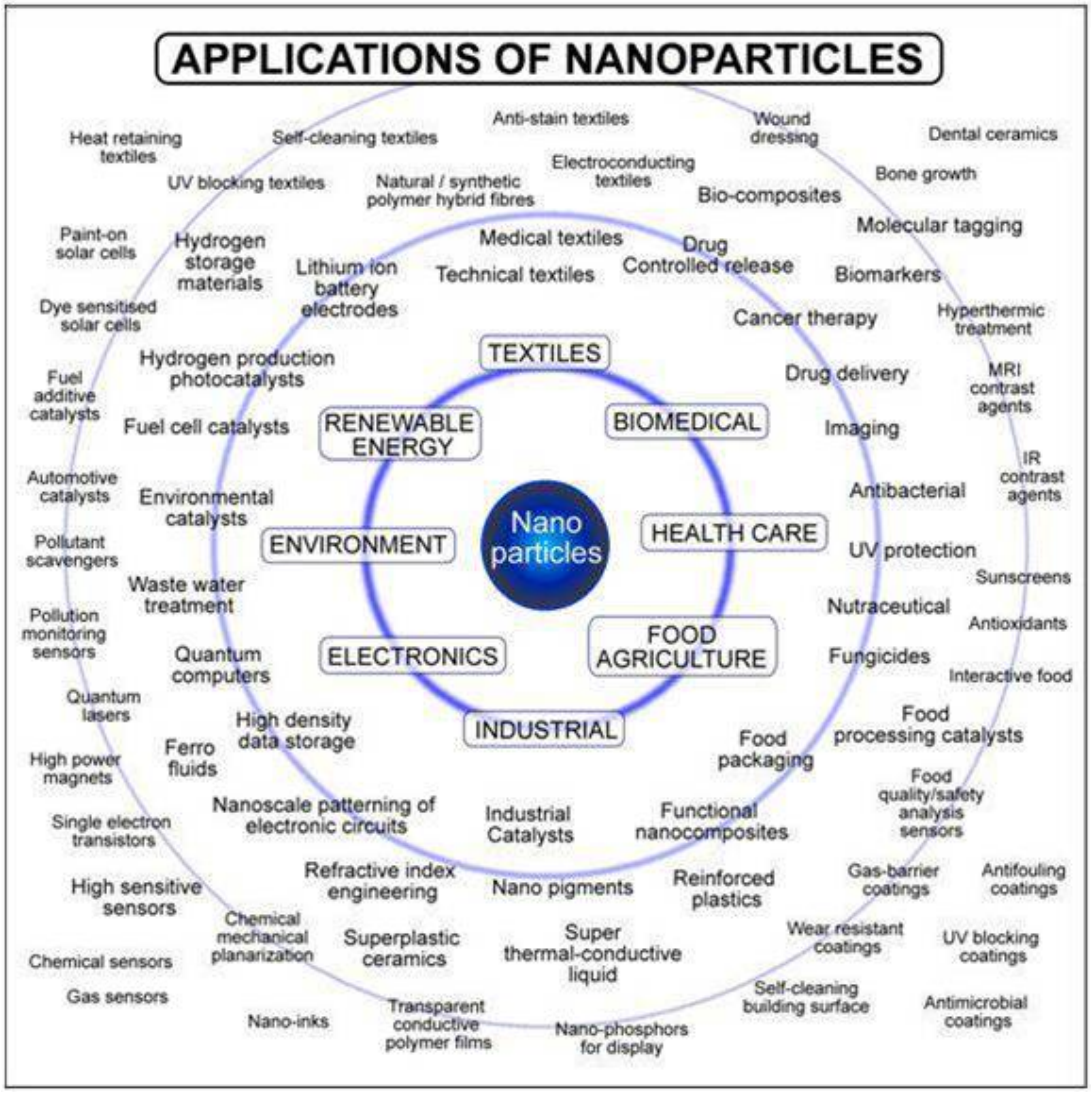

In the last three years, important research projects have been developed all over the world to explore the possibility to utilize gold or silver nanoparticles as building-blocks of a new kind of matter, called Metamaterials, showing peculiar optical properties. This work of thesis has been carried out during the NANOGOLD project ("Self-Organised Nanomaterials for tailored optical and electrical properties", Grant N°228455), funded by the European Commission during the Framework Programme 7. During this multi-disciplinary project, new self-assembling and bottom-up procedures have been developed to build metamaterials.

Entering in more detail of the performed work, chapter I is intended as a basic theoretical treatment of the main phenomena that take place when metal nanoparticles are irradiated by an external electromagnetic field. Some of the most important ones are fundamental to deal with Plasmonics.

Plasmonic resonance tunability and coupling between near-fields of gold spherical nanoparticles are the main themes investigated in this work of thesis.

To achieve this goal we have followed two lines of research.

In the first one, illustrated in Chapter III, a self-assembled Policryps periodical structure has been used as a template for a tuneable plasmonic system. The grating device is made of polymer walls alternated with channels filled in with well-aligned liquid crystal. These channels have been preventively emptied and successively infiltrated with a mixture of cholesteric liquid crystal and gold nanoparticles. The optical characterization, performed with the acquisition of VIS-NIR spectra, has been conducted during the application of external electrical fields and, successively, by changing the temperature of the structure.

In the second line, described in Chapter IV, we have exploited the elastic properties of elastomeric materials (Polidymethilsiloxane, PDMS) to modify the inter-distance between spherical gold nanoparticles deposited on the surface of a template. If gold nanoparticles are immobilized on the surface, the application of a macroscopic mechanical strain to the substrate directly correspond to a nanoscale modification of particles inter-distance. Before the acquisition of spectra, under applied or released strains, nanoparticles were preventively subjected to a growth process carried out through a nano-chemistry procedure. The combination of this growth procedure with the applied strain allows a controlled decrease of the gap existing between nano-particles. Near-fields of spherical gold nanoparticles overlap and a strong coupling takes place when these gaps are very small. The detailed investigation of the coupling between these near-fields has brought to interesting results.

I Theory

I.1 Plasmonics

Plasmonics is the branch of nano-photonics that studies how to confine the electromagnetic fields at scale lengths on the order or smaller than their wavelength.

It is based on interactions of electromagnetic fields and the electronic structure of metals.

In fact, when an electromagnetic field irradiates the cloud of conduction electrons of metal atoms, these charged particles begin to move along the direction of the wave field and the cloud undergoes (Fig.1) a displacement with respect to its original position in proximity of the nucleus. A restoring force arises from Coulomb attraction between electrons and nuclei and the result is the oscillation of the cloud with respect to the nuclear framework. This ensemble of electrons can be considered a plasma with a well-defined resonance frequency that is called plasmonic resonance.

In a metal there are three types of plasmonic[1,2] resonance: bulk plasmons, Surface Plasmon Polaritons (SPP) and Local Surface Plasmon Resonances (LSPR). For bulk plasmons, these oscillations occur at the plasma frequency and have energy:

$$E_p = \hbar\sqrt{\frac{ne^2}{m\varepsilon_0}} \qquad \text{(I.1)}$$

Bulk is referred to materials with dimensions bigger respect to the wavelength of incident light.

Surface plasmon polaritons are propagating, dispersive electromagnetic waves coupled to the electron plasma of a conductor localized at the dielectric interface.

Finally, when the plasmon resonance is confined to a particle whose size is comparable or smaller than the wavelength of light, the excitations of free conduction electrons by external electromagnetic field do not propagate. For this reason, we can call this resonance Local Surface Plasmon Resonances (LSPR). If the size of the particle is smaller than the wavelength of the impinging light, this latter one sees the particle as a dipole and in condition of resonance we have a dipolar plasmon resonance. The value of the oscillation (plasma) frequency is influenced by several parameters like density of electrons, effective electrons mass, shape and size of nanoparticles.

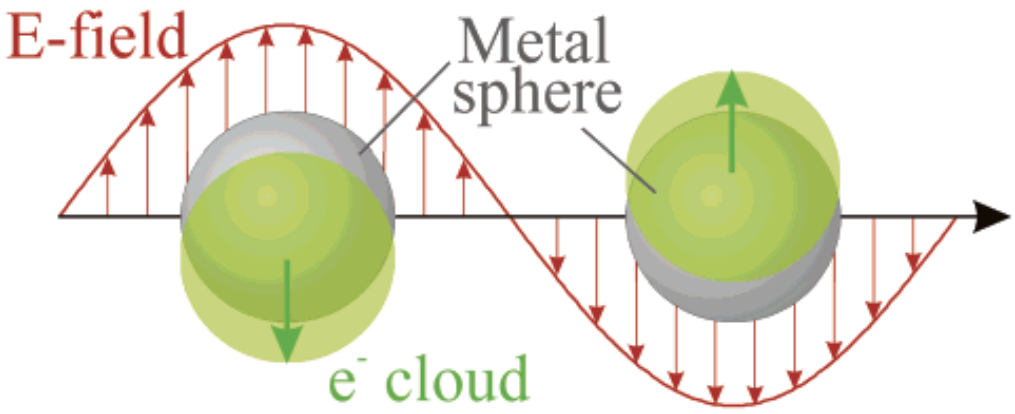

Figure 1. Schematic rappresentation of electronic displacement respect to nuclei by electric field[2]

Apart from the dipolar plasmon excitation, also higher modes as quadrupole plasmon excitation, can be considered, but only if sizes of nanoparticle begin to be comparable with wavelength. In this case, half of electron cloud moves parallel to applied field and the second half moves anti-parallel to the same field. For metals as silver or gold, electrons of d-orbitals influence the plasmon frequency.

When a nanoparticle is in resonance condition, the electric fields measured in its proximity are greatly enhanced and localized nearby the surface. Moreover, the extinction of the impinging radiation, mainly due to scattering and absorbance phenomena, shows a

maximum at this particular frequency. It can be demonstrated that this extinction strongly depends on the dielectric constant of the medium surrounding the metal nanoparticle. To relate the dipole plasmon frequency of metal nanoparticles to this parameter, we can treat the interaction between the field and the particle in a quasi-static approximation. In fact, if the sizes of spherical particles are considered much smaller than the wavelength of the electric field, $d << \lambda$ and d<100 nm, the phase of the harmonically oscillating field can be considered constant and the interaction is governed by electrostatics rather than electrodynamics. In this picture, it is possible to use the wavelength-dependent dielectric constant of the metal particle, ε, and dielectric constant of surrounding media, ε_m. If we have an homogeneous sphere of radius a localized in an uniform electrostatic field **E**=E_0**z,** and if the medium around the sphere is isotropic and non-absorbing and it has a dielectric constant ε_m, to determine the electric field around nanoparticle we must solve the Laplace equation for the potential:

$$\nabla^2 \phi = 0 \qquad \text{(I.2)}$$

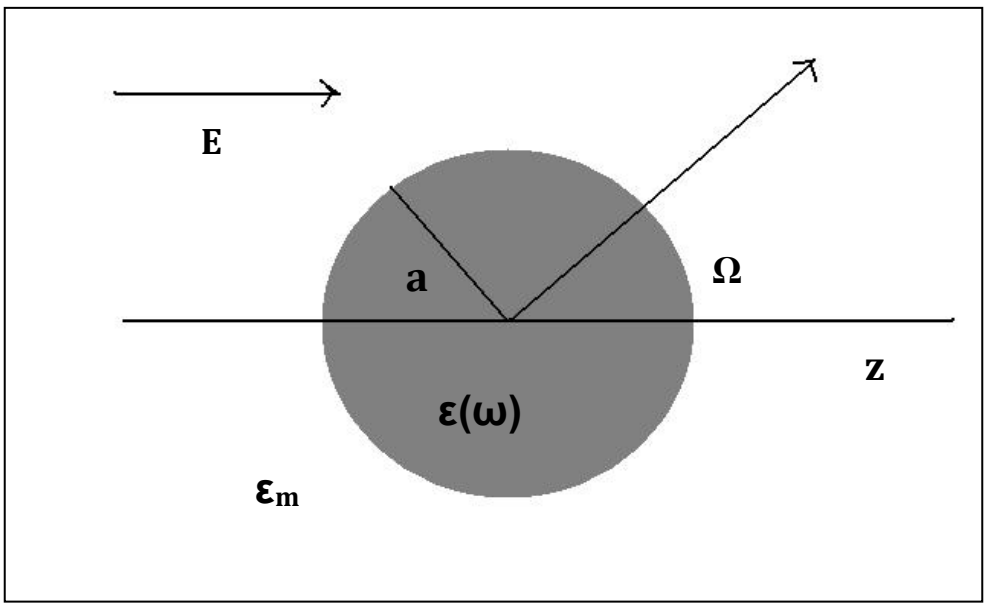

Then, from the potential it is possible to calculate the electric field:

$$E = -\nabla^2\phi \qquad \text{(I.3)}$$

To develop the solutions[1,2] we must apply the boundary conditions: i) ϕ is continuous at the sphere surface; ii) the normal component of electric displacement **D** is also continuous. At the end, we have:

$$\varphi_{in} = -\frac{3\varepsilon_m}{\varepsilon + 2\varepsilon_m} E_0 r\cos\Omega$$
$$\varphi_{out} = -E_0 r\cos\Omega + \frac{\varepsilon - \varepsilon_m}{\varepsilon + 2\varepsilon_m} E_0 a^3 \frac{\cos\Omega}{r^2} \qquad \text{(I.4)}$$

ϕ_{out} is the potential deriving from the superposition of applied field and dipole field located at the particle center. It is possible to write this potential with the dipole moment:

with **p** as:

$$\varphi_{out} = -E_0 r\cos\Omega + \frac{\vec{p}.\vec{r}}{4\pi\varepsilon_0\varepsilon_m r^3}$$
$$\vec{p} = 4\pi\varepsilon_0\varepsilon_m a^3 \frac{\varepsilon - \varepsilon_m}{\varepsilon + 2\varepsilon_m}\vec{E}_0 \qquad \text{(I.5)}$$

If we introduce the polarizability α as $\vec{p} = \varepsilon_0\varepsilon_m\alpha\vec{E}_0$, we have:

$$\alpha = 4\pi a^3 \frac{\varepsilon - \varepsilon_m}{\varepsilon + 2\varepsilon_m} \qquad \text{(I.6)}$$

The polarizability shows a resonance behaviour when the denominator $|\varepsilon + 2\varepsilon_m|$ is minimum. ε is the complex dielectric function of the metal sphere: $\varepsilon(\omega) = \varepsilon_r(\omega) + i\varepsilon_i(\omega)$. The resonance condition gives:

$$\text{Re}[\varepsilon(\omega)] = -2\varepsilon_m \qquad \text{(I.7)}$$

This is the Fröhlich condition and the associated mode is the dipole surface plasmon of the spherical metal nanoparticle.

It is worth noting that nanoparticles, excited at plasmon resonances, irradiate electromagnetic fields. If a<<λ, these fields can be considered of dipolar type. If nanoparticles are illuminated by plane waves $\mathbf{E(r,}t)=\mathbf{E_0}\exp(-i\omega t)$, a dipole moment $\mathbf{p}(t) = \varepsilon_0\varepsilon_m\alpha\mathbf{E_0}\exp(-i\omega t)$ is induced, with α calculated as above. The radiation of the dipole leads to the scattering of the plane wave interacting with the metal sphere.

A consequence of the resonantly enhanced polarization α is the enhancement of metal nanoparticle scattering (C_{sca}) and absorption (C_{abs}) cross sections:

$$C_{sca} = \frac{k^4}{6\pi}|\alpha|^2 = \frac{8\pi}{3}k^4a^6\left|\frac{\varepsilon-\varepsilon_m}{\varepsilon+2\varepsilon_m}\right|^2$$
$$C_{abs} = k\,\mathrm{Im}[\alpha] = 4\pi ka^3\,\mathrm{Im}\left[\frac{\varepsilon-\varepsilon_m}{\varepsilon+2\varepsilon_m}\right] \qquad \text{(I.8)}$$

If the particle is small, a<< λ, the efficiency of absorption is much higher than the scattering one.

These equations show that for metal nanoparticles both cross sections have a resonantly behaviour when the Frölich condition is fulfilled. When a beam probe irradiates a sphere of volume V and dielectric function $\varepsilon(\omega)$ in a medium with dielectric constant ε_m, the expression for extinction cross section $C_{ext} = C_{abs}+C_{sca}$ gives:

$$C_{ext} = 9\frac{\omega}{c}\varepsilon_m^{3/2}V\frac{\varepsilon_2}{[\varepsilon_1+2\varepsilon_m]^2+\varepsilon_2^2}. \qquad \text{(I.9)}$$

The other theory that gives the same result and also explains the red colour typical of colloidal gold nanoparticle was developed by Gustav Mie[3,4] in 1908. He solved the Maxwell's equations for an light wave interacting with small spheres. Electrodynamics calculation, with appropriate boundary conditions for a spherical object, leads to multipole oscillations for the extinction cross-section σ_{ext} and scattering cross section σ_{sca}:

$$\sigma_{ext} = \frac{2\pi}{|k|^2}\sum_{L=1}^{\infty}(2L+1)\mathrm{Re}(a_L + b_L)$$
$$\sigma_{sca} = \frac{2\pi}{|k|^2}\sum_{L=1}^{\infty}(2L+1)\left(|a_L|^2 + |b_L|^2\right) \qquad \text{(I.10)}$$

with $\sigma_{abs} = \sigma_{ext} - \sigma_{sca}$ and

$$a_L = \frac{m\psi_L(mx)\psi_L^{'} - \psi_L^{'}(mx)\psi_L(x)}{m\psi_L(mx)\eta_L^{'}(x) - \psi_L^{'}(mx)\eta_L(x)}$$
$$b_L = \frac{\psi_L(mx)\psi_L^{'} - m\psi_L^{'}(mx)\psi_L(x)}{\psi_L(mx)\eta_L^{'}(x) - m\psi_L^{'}(mx)\eta_L(x)} \qquad \text{(I.11)}$$

where m=n/n_m, with n complex refractive index of the particle and n_m is the real refractive index of the surrounding medium. k is the wave-vector, $x = |k|r$ and r is the radius of nanoparticle. ψ_L and η_L are the Riccati-Bessel cylindrical functions. L is the summation index of the partial waves. L=1 corresponds to the dipole oscillation while, L=2 is associated with the quadrupole oscillation and so on.

For nanoparticles much smaller than the wavelength of light, only the dipole oscillation contributes significantly to the extinction cross-section. The Mie theory then reduces to the expression just found before:

$$C_{ext} = \sigma_{ext} = 9\frac{\omega}{c}\varepsilon_m^{3/2}V\frac{\varepsilon_2}{\left[\varepsilon_1 + 2\varepsilon_m\right]^2 + \varepsilon_2^2} \qquad \text{(I.12)}$$

The resonance condition is

$$\varepsilon_1(\omega) = -2\varepsilon_m \qquad \text{(I.13)}$$

with ε_2 small or weakly dependent of ω. In Fig.2 we report a graphic of a typical spectrum of a surface plasmon resonance relative to gold nanoparticles with size of about 20 nm.

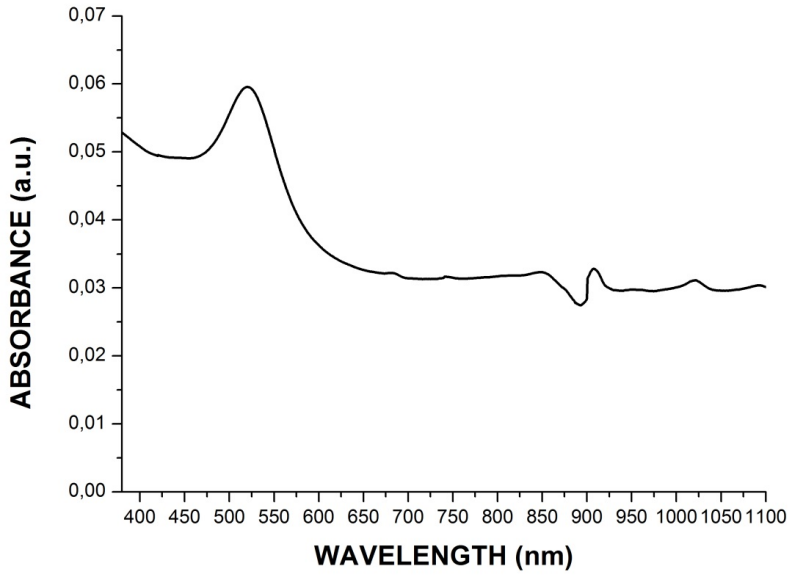

Figure 2: typical plasmon resonance of spherical gold nanoparticles with a peak at 525 nm

I.2 From macroscale to nanoscale

Matter changes significantly its properties when its dimensions are reduced from bulk (10^{-6}m) to molecular or atomic scale (10^{-10}m). Nanoscale (10^{-9}m), in this decrease of dimension (from 10^{-6}m to 10^{-10}m), is placed in intermediate sit, and for this reason, optical, mechanical and electrical properties[5,6] of nanostructures are size and shape dependent specially[6] in the range between $1< r <100$ nm.

In general, nanoparticles can be composed by semi-conductors, dielectric materials or noble-metals[4,7,8,9]. The latter, are in their neutral valence state or as oxides, sulphides etc. All particles, semi-conducting or metallic, have in common that they must be stabilized by molecules attached at their surface (to control the size and to prevent them from agglomeration and precipitation) or must be embedded in a solid matrix in order to avoid aggregation and the formation of the thermodynamically favoured bulk material. In the

absence of any counteractive repulsive forces, the Van der Waals forces between two metal nanoparticles would lead towards coagulation. This can be avoided by either electrostatic or steric stabilization[8]. In this way, for example, surface organic molecules can prevent oxidation of neutral metal in solution and small nanoparticles of gold can be isolated as a powder and are completely stable against oxidation[11]. Metallic nanoparticles can be prepared from chemical to metal vapour synthesis[10]. The most widely used and oldest method is reduction of metal salt in solution by reducing agents such a sodium citrate, phosphor, sodium borhydride or hydrogen[12].

In a nanoscale ensemble of atoms, the number of atoms located at the surface is much higher than the corresponding bulk atoms number. The same happens for electrons, which will give, as a consequence, surface effects.

In a noble metal[4], the conduction band is half-filled and the density of energy levels is so high that a noticeable separation in energy level within conduction band (intraband transition) is only observed when the nanoparticles are made up of just few atoms (N=100). The level spacing of one electron states can be approximated by E_F/N, where the Fermi energy is typically of the order of 5 eV in most metals. A 10 nm gold nanoparticle, consisting of about 30000 atoms, would therefore have an energy level spacing of only 0.167 meV. Moreover, the electrons of the conduction band (d electrons in silver and gold), can be considered as free in the material. The mean free path is about 50 nm, therefore in particles with dimension smaller than this length, no scattering is expected from the bulk, while all interaction are due to the surface. So, when the wavelength of light is much larger than the nanoparticle size electrons begin to oscillate coherently with a collective frequency and as the wave front of light passes, the electron density is polarized to one surface and then it is recalled by the opposite charge of nuclei. This oscillation has the same frequency of light, and this resonance cause a standing oscillation. The resonance condition is related to absorption, scattering, size, shape, dielectric constant of the metal

and medium surrounding the nanostructure. If size and/or shape change, there is also a change in the geometry of electrons density that causes a shift in the electric field density on the surface. A new arrangement of electrons on the surface is also related to the surrounding medium. So by changing these parameters, it is possible to tune the LSPR in wavelength and intensity. The increasing in intensity, leads to an enhancement of the electric field around nanoparticles.

I.3 Plasmonic Coupling and Plasmon Ruler Equation

I.3.1 Near Field

This strong electric field[13], induced by the exciting light, is confined to the surface of the nanoparticle, and in resonance condition, there is an enhancement of this near-field. If E_0 is the incident field at resonance frequency, the electric field on the surface of nanoparticle is given in the dipolar limit as:

$$E_{surface} = \frac{(1+k)\varepsilon_m}{(\varepsilon + k\varepsilon_m)} E_0 \qquad \text{(I.14)}$$

where k is the shape factor related to the geometry of surface (k=2 for sphere).

At resonance Re(ε)= -kε_m, and the ratio

$$\left(\frac{|E|}{|E_0|} \right)^2 \qquad \text{(I.15)}$$

has a maximum.

As it has already been written, if the typical size of the nanoparticle is smaller than the wavelength of the exciting light, absorption effects mainly due to electron-phonon interaction are prevalent. If the size increase, the scattering process starts being important. These two effects are responsible of the damping of the near-field with a radiative decay that increases with the size of the nanoparticle, because both effects are enhanced at LSPR frequency. For a particle with radius r in an electrical field E_0, the near-field at a distance r along the direction parallel to the incident light polarization, is given by the expansion in multipolar modes:

$$E_{near\,field} = \frac{2\alpha E_0}{4\pi\varepsilon_0 r^3} + \frac{3\beta \dot{E}_0}{4\pi\varepsilon_0 r^4} + \frac{4\gamma \ddot{E}_0}{4\pi\varepsilon_0 r^5} + ... \qquad \text{(I.16)}$$

where $\alpha, \beta, \gamma, ...$ are respectively the dipole, quadrupole, octupole, …. polarizability tensors of the particle. By getting closer to the particle, a reliable estimate of the near-field needs to take into account not only the dipolar contribution but also the quadrupolar and octupolar ones.

I.3.2 Coupling between near-fields

When two metal nanoparticles are close to each other, the electric field felt by each particle can be written as the sum of incident field E_0 and near-field E_{nf}. [13-16]

$$E = E_0 + E_{nf} \qquad \text{(I.17)}$$

The near-field on one particle can interact with that on an adiacent particle and this interaction between nanoentities gives the coupling of plasmonic fields with a modulation of the frequency of this last one. As a result there is a strong red-shift related to the inter distance between nanoparticles and a low energy is required to drive this coupled plasmon

resonance. This coupling effect can be exploited as basis of intense enhancement of spectroscopic signals as SERS, while through plasmon-shift is possible to meausure the distance between particles.

I.3.3 Polarization and inter-distance dependence of plasmon coupling

Several attempts have been made to provide a model that can explain the plasmonic coupling[17-20]. Su et al.[23], studying a system of elliptical gold nanoparticle pairs, observed that the plasmon shift decays exponentially as a function of the inter-particle separation.
Successively, a systematic calibration and procedure standardization has been realized sperimentally by P.K. Jain et al[13,14]. They found a rule to connect the shift induced by coupling as a function of inter distance between nanoparticles. By applying this new universal and operative method, called Plasmon Ruler equation, has been possible to describe plasmonic coupling between near-fields of nanostructures. The main result of this ruler is the independence of coupling from size of nanoparticles and the dependence only by their reciprocal gap.
This results have been obtained by studying a system of ordered coupled nano-disk put at different distance from each others. In this way it has been possible to observe a polarization dependence of the plasmon coupling. In more detail, for a polarization of the exciting light oriented along the interparticle axis, the plasmonic shift increases exponentially by decreasing the interparticle gap. A theoretical analysis shows that if the shift and gap are respectively normalized by the single-particle plasmonic wavelength and particle diameter, this exponentially behaviour results independent of the size of nanodisks. This noticeable result can be extended to nanoparticles of different shape as well as for

different dielectric media surrounding the particles[22]. Thus, at the basis of the dipolar-coupling model, there is a universal scaling behaviour of the particle-particle plasmon coupling that is a function of the interparticle distance. Given the universal character of this behaviour, it has been defined in literature as plasmon ruler. The experimental plasmon ruler equation[14] for a couple of nanoparticles is:

$$\frac{\Delta\lambda}{\lambda_0} \approx k * \exp\left(-\frac{s}{\tau D}\right) \qquad \text{(I.18)}$$

where s is the inter-particle edge-to-edge separation, D is the diameter of the particle, $\Delta\lambda / \lambda_0$ is the normalized plasmon shift. In the picture of the dipolar coupling-model, $\Delta\lambda / \lambda_0$ represents a measure of the inter-particle near-field coupling. Before to proof (I.18) we want to prove that a system of dipoles increases its polarizability when the electric field is polarized parallel rather than perpendicular to the axis between the dipoles. We start from polarizability of a particle with a not well-defined shape[13]:

$$\alpha = (1+k)\varepsilon_0 V \frac{(\varepsilon - \varepsilon_m)}{(\varepsilon + k\varepsilon_m)} \qquad \text{(I.19)}$$

where $\varepsilon = \varepsilon(\omega)$ is the wavelength dependent dielectric function of the metal the nanoparticle is made of, ε_m is the permittivity of the surrounding medium and ε_0 is the vacuum permittivity. α became maximum when $\mathrm{Re}(\varepsilon) = -k\varepsilon_m$ and if we consider a sphere, k=2. In a quasi-static approximation, an isolated particle in a electric field E_0, has a dielectric dipole μ that is given by:

$$\mu = \alpha\varepsilon_m E_0 \qquad \text{(I.20)}$$

where α is the Clausius-Mossotti dipole polarizability of an isolated nanoparticle. When there is a random distribution with high density of particles, everyone has others particles

in the neighboring and the electric field felt by each of these is the sum of the incident electric field (exciting light) and the near-field of the neighbouring particle considered as electric dipoles. If we consider a dimer of nanoparticles[13,14] in a electric field, this ones can be considered a system of coupled dipoles. In the dipolar interaction limit, the resultant field is:

$$E = E_0 + \frac{\xi \mu'}{4\pi\varepsilon_m \varepsilon_0 r^3} \qquad (1.21)$$

where ξ is the orientation factor that depends on the reciprocal alignment of the two single-particle dipoles and from the alignment of dipoles with respect to the wave field:

$$\xi = 3\cos(\theta_1)\cos(\theta_2) - \cos(\theta_{12})$$

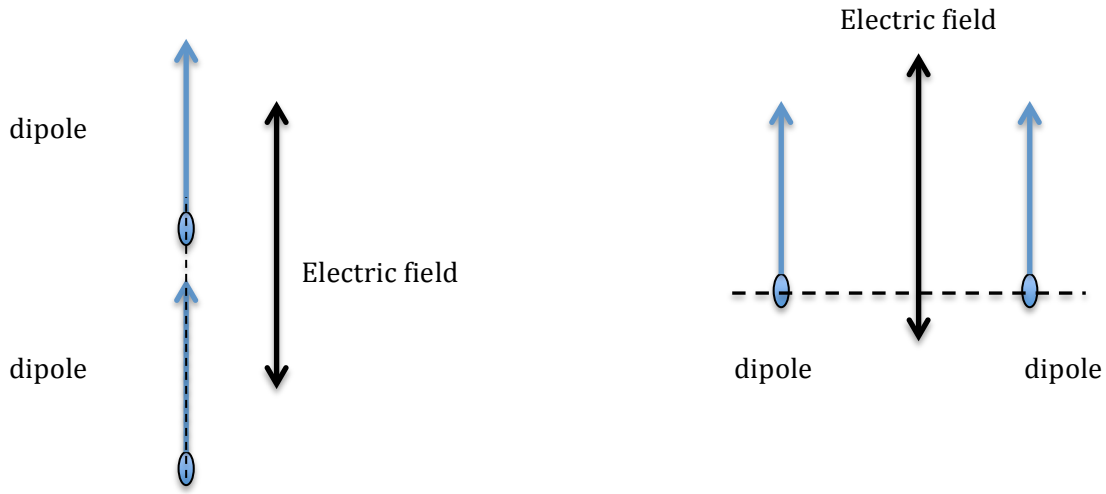

Figure 3 : in this scheme we show the two configurations of electrical field parallel to interaxis of dimer (left) and perpendicular (right)

If dipoles are parallel, the angles between both is zero $\theta_{12} = 0$ (both sides of figure); if the electric field is parallel to interaxes dipoles, the angles between dipoles and field is zero, $\theta_1 = \theta_2 = 0$ (left side of figure) and $\xi = 2$; if electric field is orthogonally to inter-axes of dipoles (right side of figure), angles between field and dipole are both 90°, and $\xi = -1$.

The relative polarizability[14,22] α' of the two-particle system is given by:

$$\alpha' = \frac{\alpha}{1 - \frac{\xi\alpha}{4\pi\varepsilon_0 r^3}} \tag{I.22}$$

and if we use the explicit expression of α (I.19) for spheres with a volume $V = \pi D^3 / 6$

I.22 became:

$$\alpha' = \frac{4\pi\varepsilon_0 (\varepsilon - \varepsilon_m) D^3}{\varepsilon\left(8 - \xi\frac{D^3}{r^3}\right) + \varepsilon_m\left(16 + \xi\frac{D^3}{r^3}\right)} \tag{1.23}$$

The maximum for polarization is obtained minimizing the denominator as :

$$\varepsilon_r = -\frac{\left(16 + \xi\frac{D^3}{r^3}\right)}{\left(8 - \xi\frac{D^3}{r^3}\right)}\varepsilon_m \tag{I.24}$$

If in this formula we introduce the gap between particles as the edge-to-edge distance defined as s=r-D (difference between center-to-center particles and one diameter), we have:

$$\varepsilon_r = -\varepsilon_m \frac{\left[16\left(\frac{s}{D}+1\right)^3 + \xi\right]}{\left[8\left(\frac{s}{D}+1\right)^3 - \xi\right]} \tag{I.25}$$

with:

$$k_{system} = \frac{\left[16\left(\frac{s}{D}+1\right)^3 + \xi\right]}{\left[8\left(\frac{s}{D}+1\right)^3 - \xi\right]} \tag{I.26}$$

For $s \to \infty$ (isolated spherical particle) we have k_{system}= k= 2 and $\varepsilon_r = -2\varepsilon_m$. If light is polarized along the inter-particle axes, we have: $\xi = 2$, and the expression (1.25) becomes:

$$\varepsilon_r\big|_{\xi=2} = -\varepsilon_m \frac{\left(8\left(\frac{s}{D}+1\right)^3+1\right)}{\left(4\left(\frac{s}{D}+1\right)^3-1\right)} \qquad \text{(I.27)}$$

If $\xi = -1$, light polarized orthogonally to inter-particle axes, in (1.25) we have:

$$\varepsilon_r\big|_{\xi=-1} = -\varepsilon_m \frac{\left(16\left(\frac{s}{d}+1\right)^3-1\right)}{\left(8\left(\frac{s}{d}+1\right)^3+1\right)} \qquad \text{(I.28)}$$

and the comparison between (1.27) and (1.28) gives:

$$\varepsilon_r\big|_{\xi=2} > \varepsilon_r\big|_{\xi=-1} \qquad \text{(I.29)}$$

So particles are much more polarized with a configuration of the external electric field polarized parallel $(\xi = 2)$ to the dipole inter-axes than the case when the electric field is polarized orthogonal $(\xi = -1)$ to dipole inter-axes.

Moreover, If the normalized gap (s/D) between particles decreases, there is also an increase of the polarizability of the electron cloud which is due to the attractive coupling between the neighbouring dipoles in the head to tail configuration for $(\xi = 2)$.

Utilizing the dipole approximation, the spherical shape of nanoparticles and the parallel direction of wave field along the interaxis of dimer, we can find the theoretical justification of I.18[14]. Utilizing the near-linear dependence of ε_r on wavelength in the visible (500-700 nmm) region for gold:

$$\lambda = 464,6 - 14.3\varepsilon_r \tag{I.30}$$

and get:

$$\lambda_{\max} = 464.6 + 14.3 \cdot k\varepsilon_m \tag{I.31}$$

For $(s/D) \to \infty$ k=2 and the single particle resonance wavelength maximum will be:

$$\lambda_0 = 464.6 + 28.6\varepsilon_m \tag{I.32}$$

The absolute shift, in this way, will be:

$$\lambda_{\max} - \lambda_0 = 14.3 \cdot (k-2)\varepsilon_m \tag{I.33}$$

For $\xi = 2$ utilizing the result in I.26, we can write:

$$k - 2 = \frac{3}{4\left(\frac{s}{D}+1\right)^3 - 1} \tag{I.34}$$

and at the end, by combining the I.32, I.33, and I.34 we have that the relative shift is:

$$\frac{\Delta\lambda}{\lambda_0} = \frac{42.9\varepsilon_m}{(464.6 + 28.6\varepsilon_m)} \frac{1}{4\left(\frac{s}{D}-1\right)^3 - 1} \tag{I.35}$$

This equation, where $\Delta\lambda / \lambda_0$ is a rational function of s/D, can be approximated very nearly to an exponential decay function, as I.18.

I.3.4 Dipole-dipole potential energy

In a system made of two nanoparticles with their associated dipoles, each dipole μ, is exposed to the electric field of the impinging beam E_0, and to the near-field due to the neighboring dipoles. As such, the total electric field can be written as:

$$E = E_0 + \frac{\xi\mu}{4\pi\varepsilon_0 r^3} \qquad \text{(I.36)}$$

The two dipoles system, has a potential energy[13] given by:

$$U = -\frac{\xi|\mu|^2}{4\pi\varepsilon_0 r^3} \qquad \text{(I.37)}$$

with $\xi = 3\cos(\theta_1)\cos(\theta_2) - \cos(\theta_{12})$, $\theta_1 = \theta_2 = \theta$ (dipoles are polarized with the same polarized beam), $\theta_{12} = 0$, (dipoles are aligned to the polarized beam).

From equation (1.37), we understand that if the beam is polarized along the inter-particles axis, $\theta = 0, \xi = 2$ and U<0: interaction is attractive for dipoles aligned symmetrically and there is a red-shift of plasmon resonance. If the beam wave-vector is orthogonally to inter-particle axis, $\theta = 90°$, $\xi = -1$ and U>0: in this case, interaction is repulsive between dipoles and there is a blue-shift in plasmon resonance.

I.4 Reference

1. Stefan A. Maier, ***Plasmonics: Fundamentals and Applications*** © 2007 Springer Science+Business Media LLC ISBN 978-0387-33150-8
2. K.L. Kelly, E. Coronado, L.L. Zhao, G.C. Schatz, J. Phys. Chem. B 107 (2003) 668
3. G. Mie, Ann. Phys. 25 (1908) 377.
4. S. Link, M.A. El-Sayed, Int. Rev. Phys. Chem. 19 (2000) 409.
5. U. Kreibig, V. Volmer, **Optical Properties of Metallic Cluster**, © Springer-Verlag-Berlin Heidelberg 1995
6. M. Quinten, **Optical Properties of Nanoparticle Systems**, © 2011 Wiley-VCH Verlag & Co. KGaA Boschstr. 12, 69469 Weinheim, Germany
7. Al i v i s a t o s , A. P., 1996, *J. phys. Chem.*, **100**, 13 226
8. He a t h , J. R., and Sh i a n g , J. J., 1998, *Chem. Soc. Re*Š ., **27**, 65
9. We l l e r , H., 1993, *Angew. Chem.*, *Int. Edn Engl.*, **32**, 41
10. Sc h m i d , G., 1994, *Clusters and Colloids : From Theory to Application* (Weinheim: VCH).
11. Br u s t ,M.,Wa l k e r , M., Be t h e l l , D., Sc h i f f r i n , D. J., and Wy h n m a n , R., 1994, *J. chem. Soc.*, *chem. Commun.*, 801.
12. Ha n d l e y , D. A., 1989, *Colloidal Gold: Principles*, *Methods*, *and Applications*, Vol. 1 (New York: Academic Press).
13. P.K. Jain, M.A. El Sayed, Chemical Physics Letters 487 (2010) 153-164
14. P.K. Jain, W. Huang, M.A. El Sayed, Nano Letters 2007 Vol. 7 No.7 2080-2088 and Supporting Information
15. M.K. Kinnan et al., *J. Phys. Chem. C* 2009, 113, 7079-7084

16. M.K. Kinnan and George Chumanov, *J. Phys. Chem. C* 2010, 114, 7496-7501
17. Lee, K.-S.; El-Sayed, M. A. *J. Phys. Chem. B* **2006**, *110*, 19220
18. Reinhard, B. M.; Siu, M.; Agarwal, H.; Alivisatos, A. P.; Liphardt, J. *Nano Lett.* **2005**, *5*, 2246–2252
19. Sih, B. C.; Wolf, M. O. *J. Phys. Chem. B* **2006**, *110*, 22298–22301.
20. Malynych, S.; Chumanov, G. *J. Opt. A: Pure Appl. Opt.* **2006**, *8*, S144– S147.
21. Jain, P. K.; Huang, X.; El-Sayed, I. H.; El-Sayed, M. A. *Plasmonics* **2007**, *2*, 107–118
22. P.K.Jain and M.A. El-Sayed NANO LETTERS 2008 Vol. 8, No. 12 4347-4352
23. K.H. Su, Q. Wei, X. Zhang, J.J. Mock, D.R. Smith, S. Schultz, Nano Lett. 3 (2003) 1087.

II MATERIALS

II.1 Liquid crystals

The states of aggregation of matter are classically three: solid crystal phase, liquid isotropic phase and gaseous isotropic phase. To these ones, it needs to be included the isotropic glassy phase. In the middle of 1800, others phases were discovered, called mesophases, that have intermediate properties between crystal and liquid phases. These mesophases are due to the geometric shape of their molecules so there are molecular crystals and liquid crystals. The first ones have organic molecules with globular shapes; the second ones have organic molecules with a strong asymmetry: shapes like rods, discs or bananas. Liquid crystals can be divided in thermotropic and lyotropic. The first ones transit in different types of mesophase with temperature. The second ones change phase with temperature and with concentration of liquid crystal in solvent.

Our interest is for thermotropic liquid crystals, particularly nematics and cholesterics.

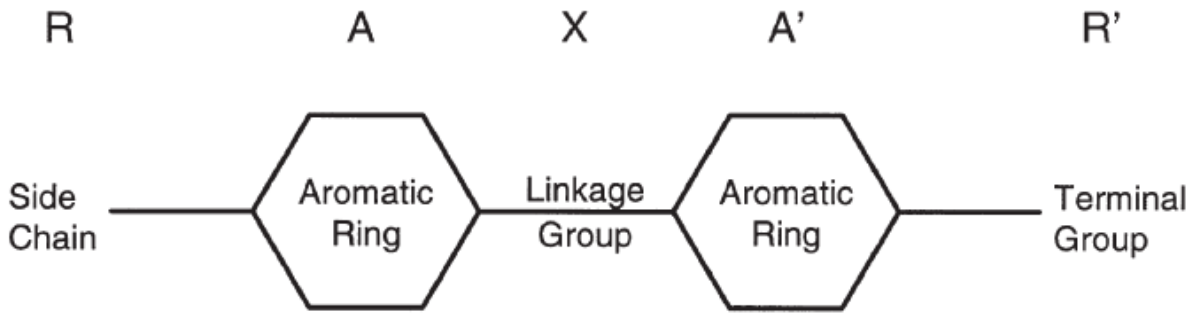

Figure 1. Molecular structure of a liquid crystal

• Nematic Liquid Crystal

In case of Nematic Liquid Crystals (NLC)[1], the centres of gravity of the molecules have no long-range order. However, there is some order in the direction of the long axes of the molecules; they tend to be parallel to some common axis called director **n** and respect to this one, molecules are center-simmetric**:** physical properties do not change for directors inversion. The **n** vector, in a polar reference system, is characterized by colatitude angle θ and azimuthal angle φ. The order of nematic phase can be estimated by utilizing a parameter S, called order parameter, with values in the range 0< S < 1 (S=0 nematic is in isotropic phase, S=1 the phase is nematic). In a sample of nematic liquid crystal, the director is not constant all over the volume. Its orientation changes firstly at the edge and then also if there are externally applied electrical fields. Typical distance where order parameter changes is in the micro-meter scale, while the typical molecular length is of the order of tens of nanometers. So, the director can be treated as a continuous function of coordinates. Once the direction of the director is clear, the macroscopic behaviour of nematics is known. For a NLC, it is possible to show that the density of free energy due to a mechanical distortion is:

$$F_d = \frac{K_1}{2}\left(\nabla \cdot \hat{n}\right)^2 + \frac{K_2}{2}(\hat{n}\cdot \nabla \times \hat{n})^2 + \frac{K_3}{2}(\hat{n}\times \nabla \times \hat{n})^2 \qquad \text{(II.1)}$$

with K_1, K_2, K_3 elastic constants named: splay, twist and bend and magnitude about 10^{-12} N. When nematics is in electrical field, the resultant of interactions is the sum of electrical and elastic ones. Optical properties of nematics are linked to its anisotropic configuration, to optical constants as dielectric constant and refractive index. Dielectric constant can be written as a tensor:

$$\varepsilon_{ij} = \varepsilon_{\perp}\delta_{ij} + \Delta\varepsilon n_i n_j \qquad \text{(II.2)}$$

with $\Delta\varepsilon = \varepsilon_{\perp} + \varepsilon_{II}$ and $\varepsilon_{\perp}$ and ε_{II} are the dielectric constants when the electric field is respectively orthogonal and parallel to director.

As the director changes locally, the same way also changes the two dielectric constants and consequently the two refractive indexes. While propagating in nematics, light meets two refractive indexes because the medium is birefringent. The effective refractive index can be written as:

$$n_{eff} = \frac{n_0 n_e}{\sqrt{n_e^2 \cos^2\theta + n_0^2 \sin^2\theta}} \qquad \text{(II.3)}$$

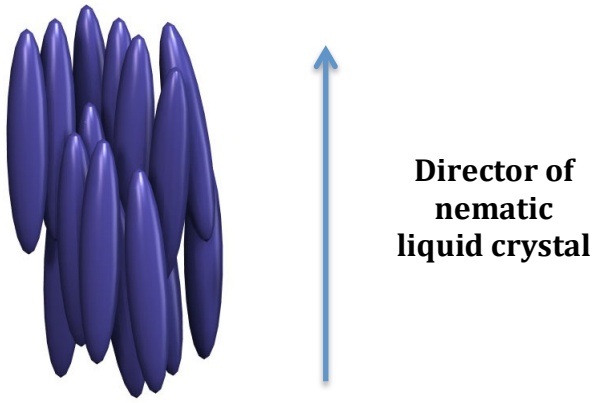

Figure 2. Schematic picture of a NLC.

• Cholesterics

A Cholesteric liquid crystal[2] is a mixture of a nematic phase and a chiral agent. The new phase has a helical structure with a periodic pitch. Locally, a cholesteric is very similar to a nematic. However, the director **n** is not constant in space; in fact it has a helical conformation and if z is the helical axis, n has thee component:

$$\begin{aligned} n_x &= \cos(q_0 z + \Phi) \\ n_y &= \cos(q_0 z + \Phi) \\ n_z &= 0 \end{aligned} \qquad \text{(II.4)}$$

where z and Φ are arbitrary. The pitch is $p_0 = 2\pi / q_0$ and the sign of q_0, pitch wave vector, distinguishes between right and left-handed helices. The pitch depends on temperature, pressure, chemical contaminants. Moreover, cholesteric is very sensitive to applied external fields. For a free distortion the free energy of cholesteric liquid crystal is given by:

$$F_d = \frac{K_1}{2}\left(\nabla \cdot \hat{n}\right)^2 + \frac{K_2}{2}(\hat{n} \cdot \nabla \times \hat{n})^2 + \frac{K_3}{2}(\hat{n} \times \nabla \times \hat{n})^2 \qquad \text{(II.5)}$$

that is the same of nematics.

Cholesteric liquid crystal can be considered an uniaxial crystal if its pitch doesn't change with external perturbation as electric field, magnetic field or optical field. The anisotropy of this material is pitch dependent, and so also those parameters that define this propertie as dielectric constant $\Delta\varepsilon = \varepsilon_{II} - \varepsilon_{\perp}$, electric conductivity $\Delta\sigma = \sigma_{II} - \sigma_{\perp}$, magnetic susceptibility $\Delta\chi^m = \chi^m_{II} - \chi^m_{\perp}$ and so on. If we apply an electric field along z (respect to helical axe), the field sees the orthogonal components of these parameters while, if the field is orthogonal to the axis, it sees the average of orthogonal and parallel components :

$$\tfrac{1}{2}(\varepsilon_{\perp} + \varepsilon_{\parallel}), \tfrac{1}{2}(\sigma_{\perp} + \sigma_{\parallel}), \tfrac{1}{2}(\chi_{\perp} + \chi_{\parallel}) \qquad \text{(II.6)}$$

As in nematic phase, if we apply an electric or in magnetic field to cholesteric liquid crystal, in the exspression of free energy we must consider respectively additional terms:

$$F_{el} = -\frac{1}{2}\Delta\varepsilon(\hat{n} \cdot \overline{E})^2 \qquad \text{(II.7)}$$

$$F_{mag} = -\frac{1}{2}\Delta\chi^m(\hat{n} \cdot \overline{H})^2 \qquad \text{(II.8)}$$

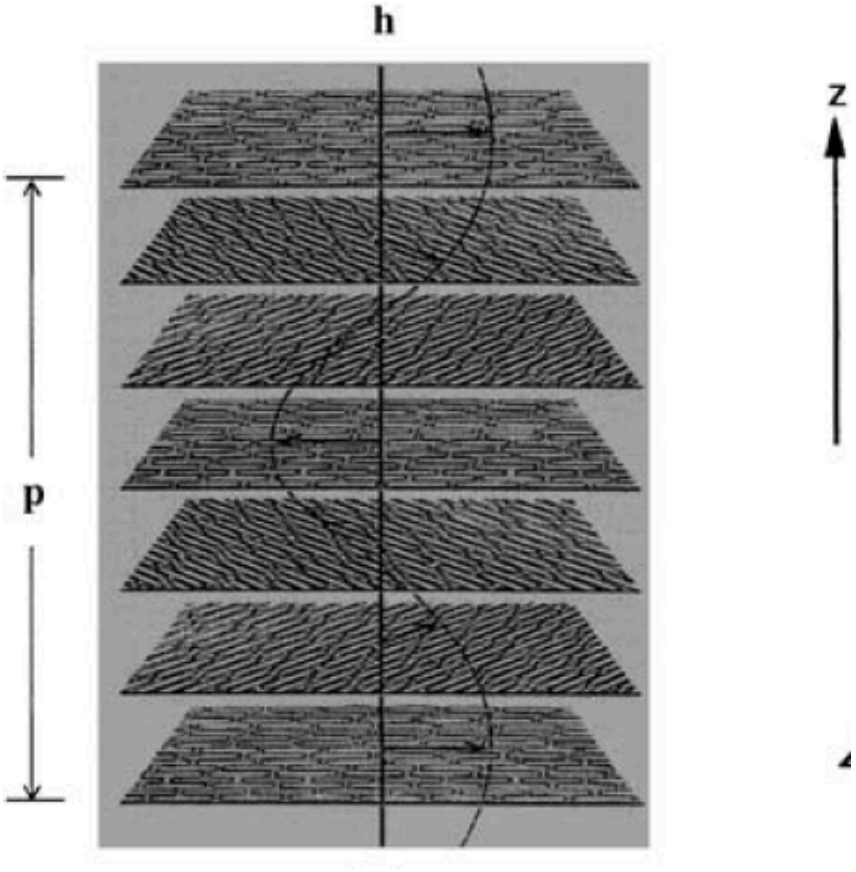

Figure 3. Helical arrangement of the director axis in a cholesteric liquid crystal; **p** is the pitch and **h** is the helix direction

II.2 Policryps

POLICRYPS[3,4,5] (acronym derived from POL(ymer) – LI(quid) CRY(stal) – P(olymer) S(lices)) indicates a micro-structure made of slices of pure polymer alternated to films of pure nematic liquid crystal, whose director is uniformly aligned perpendicularly to the polymeric slices; samples are obtained by carrying out a holographic photo-polymerization of a homogeneous syrup of LC, monomer and curing agent. The main steps for the fabrication of a POLICRYPS (transmission) holographic grating are briefly illustrated in the following, along with its performances. A homogeneous syrup of NLC, monomer and a photoinitiator is heated above the nematic–isotropic transition temperature of the NLC

component; the sample is then ‘cured’ with the interference pattern of a UV radiation. After the curing process has come to an end, the sample is slowly cooled down to room temperature, below the isotropic–nematic transition point. In Fig.1 we show a typical polycryps structure.

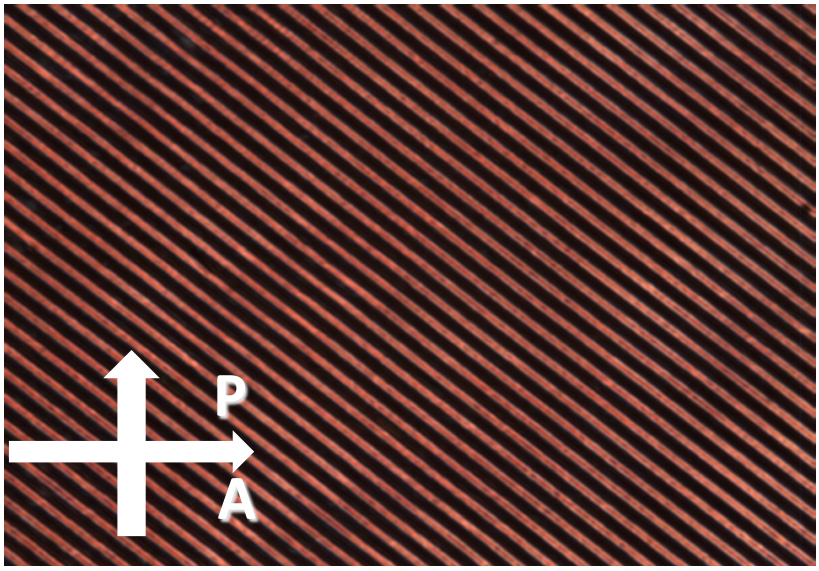

Figure 4. Polycryps structure: black stripes are the liquid crystal channels while, red stripes are the polymer walls. Image was acquired with polarizer microscope with sample between cross polarizer.

In particular, geometrical conditions determine (in the range 0.2 ÷ 15μm) the spatial periodicity of the realized sample, which can be utilized for transmitting, diffracting or reflecting an impinging light beam, with negligible scattering losses. The spatial modulation of the refractive index (from polymer to NLC) can be switched ON and OFF both by applying an electric field of few V/μm or, in some cases, by irradiating the sample with a light beam of suitable wavelength. This electrical/optical tunability is responsible for a series of distinctive characteristics of the optical effects produced by the structure, and determines the range of possible applications. This electrical/optical tunability is responsible for a series of distinctive characteristics of the optical effects produced by the structure, and determines the range of possible applications. In fact, in different

geometries, the POLICRYPS can be exploited as a switchable holographic grating, a switchable optical phase modulator, a switchable beam splitter, a tuneable Bragg filter or it can be exploited as an electro-optical edge filter in an optical interrogation system.

The above described 'single step' POLICRYPS fabrication procedure has been recently implemented in a new 'multi-steps' protocol[3] which enables both realization of an excellent morphology and the possibility of putting any kind of liquid crystalline material between the polymeric slices. After the 'usual' first step is completed with a low quality, low cost NLC, an etching process of the sample is carried out, without opening the cell, by immerging it in a water solution of tetrahydrofuran (THF); in this way, the solvent washes out the NLC from the polymeric structure by capillary flow. The process takes place above the nematic–isotropic transition temperature of the NLC (65°C), thus ensuring a low viscosity of this component, and, for short time intervals (3–4 h), the THF acts as a selective agent, removing the NLC and any eventual un-polymerized component, without affecting the regularity of the polymer slices. In Fig. 5, the sample appears to be made of sharp polymer slices separated by empty channels; this is a clear confirmation that the NLC has been completely removed.

Always in fig. 5, different optical microscope pictures show the sample during the emptying process. The micrograph in Fig.5a was acquired between cross polarizers before immerging the sample in the solvent; Fig 5b shows a sample removed from the solvent after 1 hour and Fig. 5c after 2 hours. The completely black area in Fig. 5d confirms that the LC has been completely washed out if removal of the sample from the solvent is made after 3 hours. Peculiar capabilities of the "empty POLICRYPS" structure have been investigated by observing self-organization processes in different LC phases as Nematics, for all-optical grating realization purposes, cholesterics, for optical activity features, chiral smectics, for ferroelectric fast switching.[5]

In our work, after preparing a Policryps structure as described above, we filled in its

channels with a mixture of cholesterics and gold nanoparticles. The detailed procedure and performance of the obtained system are described in chapter 3.

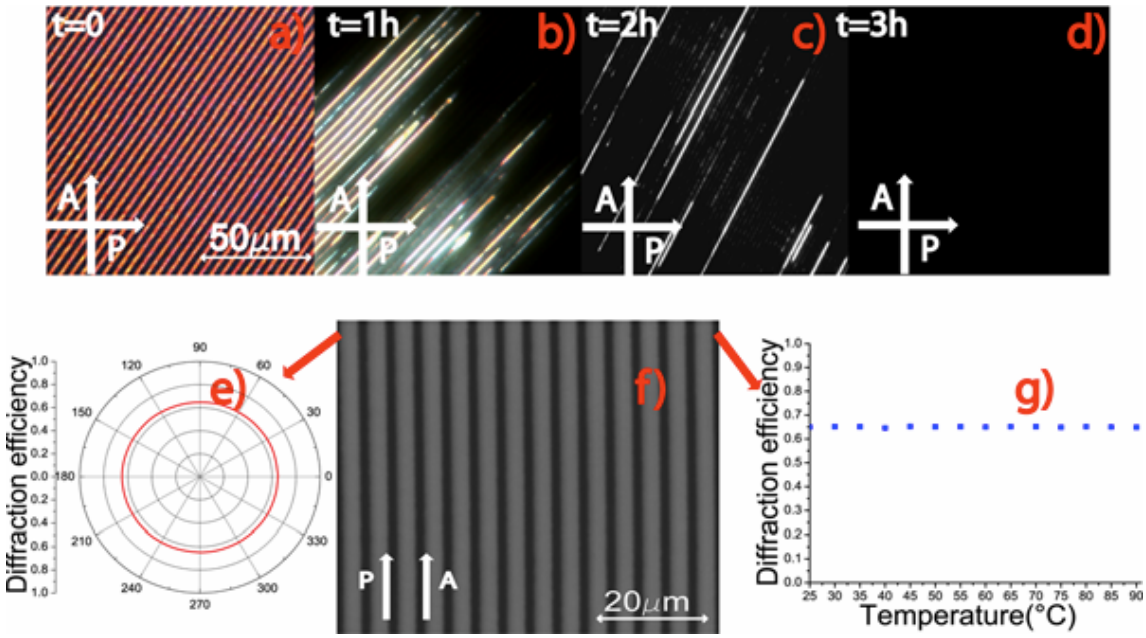

Figure 5: POM view of the POLICRYPS structure during the micro-fluidic etching process at different time scale (a-d). Polymer template after removing the NLC (f); the flat diffraction efficiency behavior versus the impinging probe polarization (e) and temperature (g) demonstrates the absence of LC in the sample.[3]

II.3 Elasticity[6,7]

In Hooke's law is established that, in matter or in structures, strain is proportional to stress applied. Dimensionally, stress is a pressure, in fact it is defined as a force applied above a unitary surface:

$$\sigma = \frac{P}{A} \qquad \text{(II.9)}$$

Strain is defined as:

$$\varepsilon = \frac{\delta l}{L} \qquad \text{(II.10)}$$

where L is the length of a material, and δl is the change of length in the direction of applied stress.

Every material has its proper stiffness. Thomas Young showed that the total strain of a structure, that must resist to an applied stress is due to stiffness effects and at the same time also to size and shape. He established a law where stress is related to strain:

$$\text{E (Young's modulus)} = \frac{\sigma}{\varepsilon} \qquad \text{(II.11)}$$

where σ is the applied stress and ε is the strain of the structure. Young's modulus is also a pressure. A material that behaves as II.11 in tension and compression is called Hookians or elastic material. From II.9, II.10 and II.11, it is possible to calculate the elastic constant of the material as:

$$k = E\left(\frac{A}{L}\right) \qquad \text{(II.12)}$$

This treatment is valid for a mono-dimensional material: strain is oriented parallel to the direction of the stress. But if we consider a tridimensional material, perpendicularly to the direction of the stress, there are two compressions. Related to this observation is Poisson's law. If ε_1 is the strain along x axis, ε_2, ε_3 are the compressions along y and z axis which can be written:

$$\varepsilon_2 = \varepsilon_3 = -\nu\varepsilon_1 = -\nu\frac{\sigma_1}{E} \qquad \text{(II.13)}$$

The proportionality constant ν is called Poisson's coefficient. The sign of compression is opposite to the strain one. From simple mass conservation principles, it can be deduced that Poisson's coefficient for an elastic material is 0.5. This is also the case of Poly(dimethysiloxane).

II.3.1 Poly(dimethylsiloxane) (PDMS)[8]

PDMS is a polymeric material with elastic behaviour or an elastomeric material. It has a tuneable Young's modulus around 750 kPa, it is optically transparent from 240 to 1100 nm and has a refractive index of 1.41. It has negligible birefringence. It has many interesting features that make it convenient for technological uses: it is compatible with many optical methods for detection, it is bio-compatible and permeable to gas and impermeable to water. Moreover, respect to glass and silicon, it is quite easy to fabricate.

PDMS consists of repeating $-OSi(CH_3)_2-$ units; the CH_3 groups make its surface hydrophobic.

The surface can be made hydrophilic by exposure to a plasma air flow: the plasma oxidizes the surface to silanol (Si-OH) and destroys methyl groups $Si-CH_3$. The plasma-oxidized surface remains hydrophilic if it stays in contact with water or polar organic solvents. In air, rearrangements occur within 30 min. The silanol groups on the surface of PDMS allow it to react with a wide range of silanes (Si-R) that are terminated with important functional groups as NH_2, COOH, SH. By silanizing an oxidized PDMS substrate with an amino-terminated silane (aminopropyltriethoxysilate) provides an electrostatic reactive surface. PDMS is compatible with water and most polar organic solvents; it swells in nonpolar organic solvents, and will absorb nonpolar solutes from aqueous solutions. PDMS is an electrical and thermic insulator and it is stable up to 300°C. Moreover, it has a low surface free energy ~20 erg/cm^2.

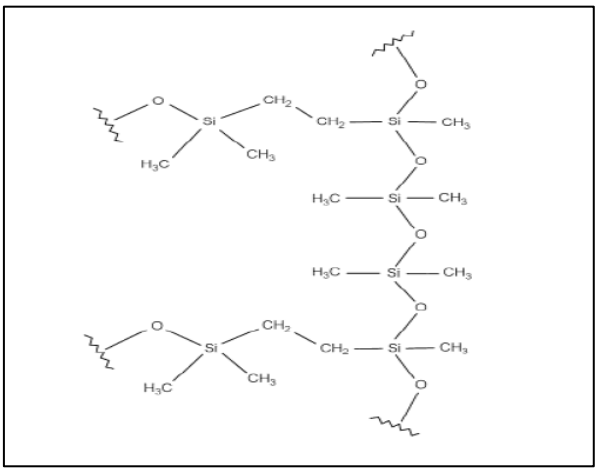

Figure 6: molecular structure of PDMS

The PDMS material used in our experiments is the Sylgard 184 Elastomeric Kit (*Dow Corning Corp.*) and it contains a base polymer (part A) and a curing agent (part B). The ways of mixing the two parts are several; we used a ratio 10:1, and they were first mixed thoroughly and then dispersed in a petri-dish. The liquid layer was exposed to air in a controlled room so to degas and to eliminate air bubbles. Then, the petri-dish with the liquid PDMS was introduced in a oven and cured at 80°C for 1 hour. At the end of the curing time, the vessel was extracted and the solid PDMS was peeled off and cut so to obtain the template of the sample.

Both curves in fig. 7a, show a linear regime up to a strain of 45%, which correspond, particularly, to a constant elastic modulus of 1.76MPa for Sylgard 184. In fig. 7b, in the same range of strain elastic modulus is constant.

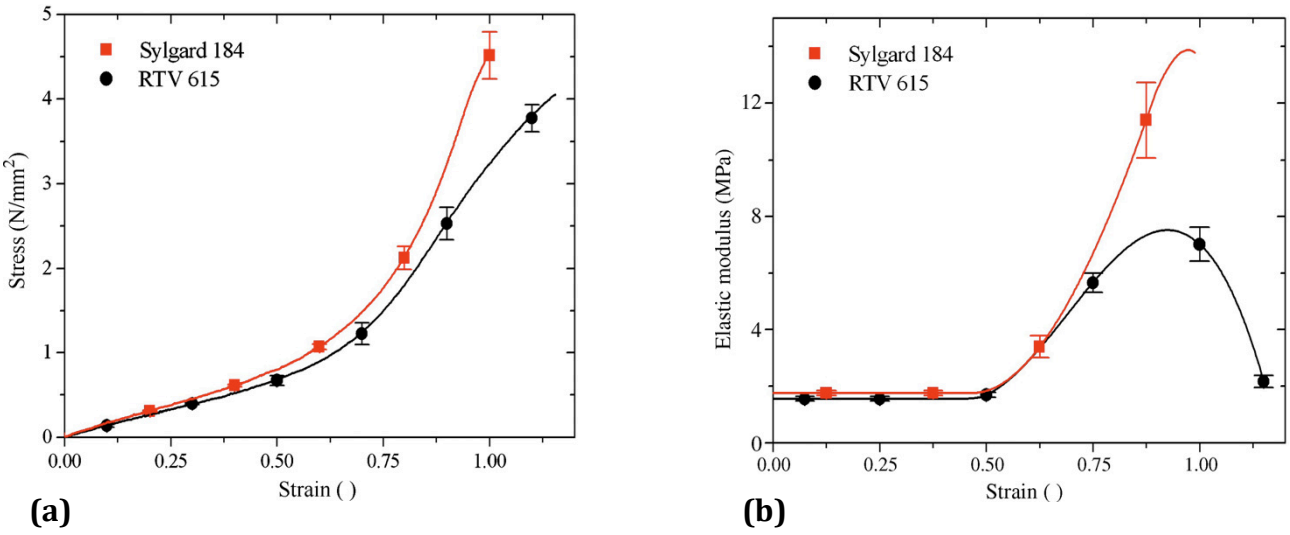

Figure 7. Stress-strain diagram and Elastic mod. vs strain of RTV and Sylgard 184[9]

In the same article the optical dispersion of Sylgard 184 was measured. The refractive index decreases by increasing the probe wavelength, which is typical for glass and polymeric materials. Dispersion along the whole visible range is well described by the Sellmeier's empirical relationship:

$$n(\lambda)^2 = 1 + \frac{B_1\lambda^2}{\lambda^2 - C_1} + \frac{B_2\lambda^2}{\lambda^2 - C_2} + \frac{B_3\lambda^2}{\lambda^2 - C_3} \qquad \text{(II.14)}$$

B_1, B_2, B_3, C_1, C_2, C_3 are experimentally determined Sellmeier coefficients.

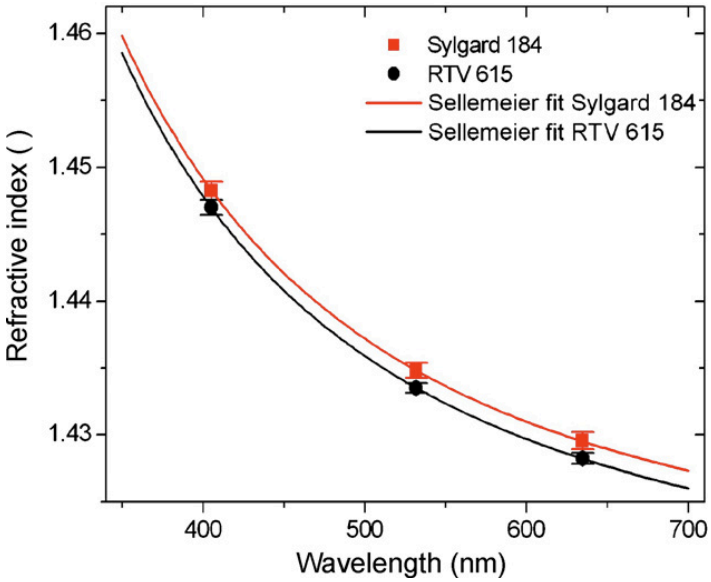

Figure 8. Optical dispersion of Sylgard 184[9]

II.4 Spherical Gold Nanoparticles

II.4.1 Synthesis[10-13]

New photonic properties of noble metals were discovered when the nanoscale limit for particles fabrication was broken. Mainly, methods to produce nanoparticles can be classified into gas-phase and liquid-phase ones. Among the latter ones, the simplest procedure to synthetize silver or gold nanoparticles is the trisodium citrate reduction of tetrachloroauric acid ($HAuCl_4$). This one is well-known in literature as the Turkevich method[9-12], that was successively refined by Frens[12].

Using this procedure, trisodium citrate has the double function to reduce the auric acid and to cap the particles so to avoid clusterization. With Turkevich method, it is possible to produce monodisperse spherical nanoparticles with diameters in the range $17 < d < 90$ nm in deionized water. During the nucleation process, gold ions Au^{3+} are produced and then reduced by citrate in atoms of Au^0 that, at this point, begin to aggregate. Then, a growing

process takes place, where the gold ions are reduced in neutral atoms on the surface of these nuclei, increasing their size. To control the size, it is very important the concentration of citrate that, in this phase of the synthesis, caps the nanoparticle. The procedure described below is the one applied in our experiment.

The ingredients are: Milli Q-water (18,2 MΩ-cm); hydrogen tetrachloroaurate (III) ($HAuCl_4$) was purchased from Alfa Aesar; sodium citrate tribasic dehydrate that was purchased from Sigma-Aldrich. GNPs were prepared in Milli Q-water according to the well known Turkevich method[10-13]: 500 mL of a 0.25 mM solution of $HAuCl_4$ in a vessel under constant magnetic stirring was heated to 100°C in an oil bath. When the solution began to boil, 12.5 mL of 0.03 M sodium citrate was added. The solution, during the 15 min of reaction, changed colour (from black to red wine). At the end the reaction vessel was removed from the oil bath and was left to cool to room temperature. TEM images show the spherical shape and size of colloidal nanoparticles and spectrum acquired on the same colloidal solution give a dipolar plasmon resonance as $\lambda = 520\,nm$.

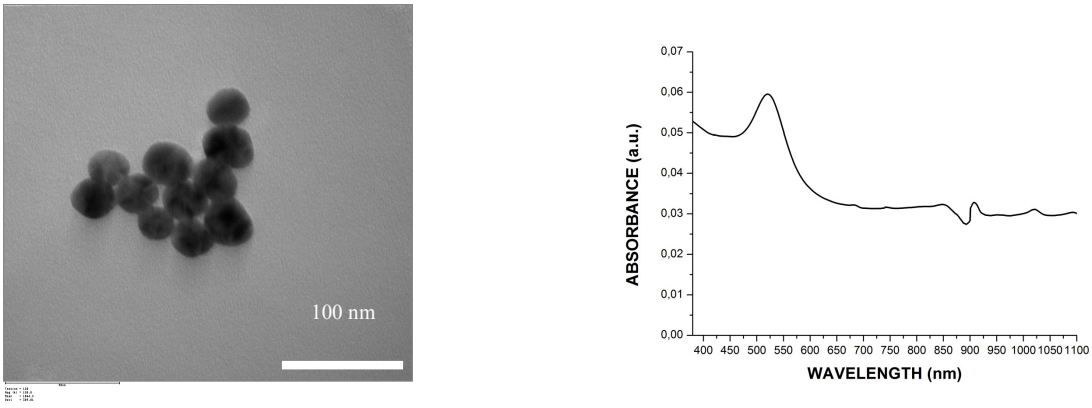

Figure 9. TEM image of spherical colloidal gold nanoparticle and related spectrum

II.4.2 Increasing the size of GNPs: seeding growth process.[14-17]

Gold nanoparticles produced by reducing procedures, as Turkevich method[10-12], give good results for obtaining little range of sizes. To tailor and control much more shapes and sizes of noble metal nanoparticle, it is possible to use the seeding growth self-assembling technique[14-17]. By applying this technique, it is possible to deposit gold atoms on the surface of bulk gold by using hydroxylamine (NH_2OH) to reduce Au^{3+} in Au^0 [14-17]. We chose this method, because it is very simple to handle and avoids new nucleation of gold nanoparticles. This happens because the kinetics for NH_2OH reduction of adsorbed Au^{3+} greatly exceeds the rate of the solution reduction[16]. Moreover, this method is consistent, reproducible and furthermore the process works at room temperature[15]. The scheme of this procedure is reproduced below[14]:

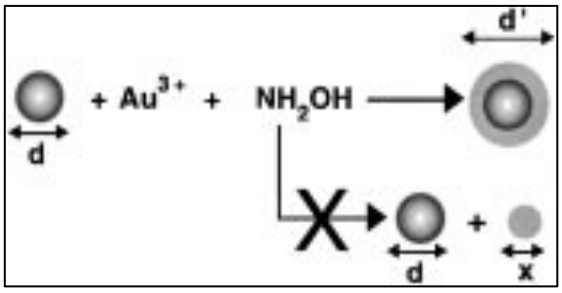

Figure 10. Diagram rappresentative of growing process

The reduction process is accelerated by catalytic action of nanoparticles gold surface; so all gold ions tend to increase the size of particles. The seeding approach can be applied both to gold colloidal seeds and with surface-confined nanoparticles. The first approach, gives not only an increasing of size but also an improving of the monodispersity. While utilizing the second one, there is the possibility to initially fix density and (center-to-center)

inter-distance of particles seeds above the surface of a PDMS template. Then, by repeating several steps of growth, it is possible to decrease the gap (edge-to-edge distance) between nanoparticles, leaving unchanged their inter-distance. On this way, cycle after cycle of growth, nanospheres approach each other and their near-fields begin to couple.

The procedure followed will be illustrated in more detail in chapter 4 where it is described the fabrication of sample.

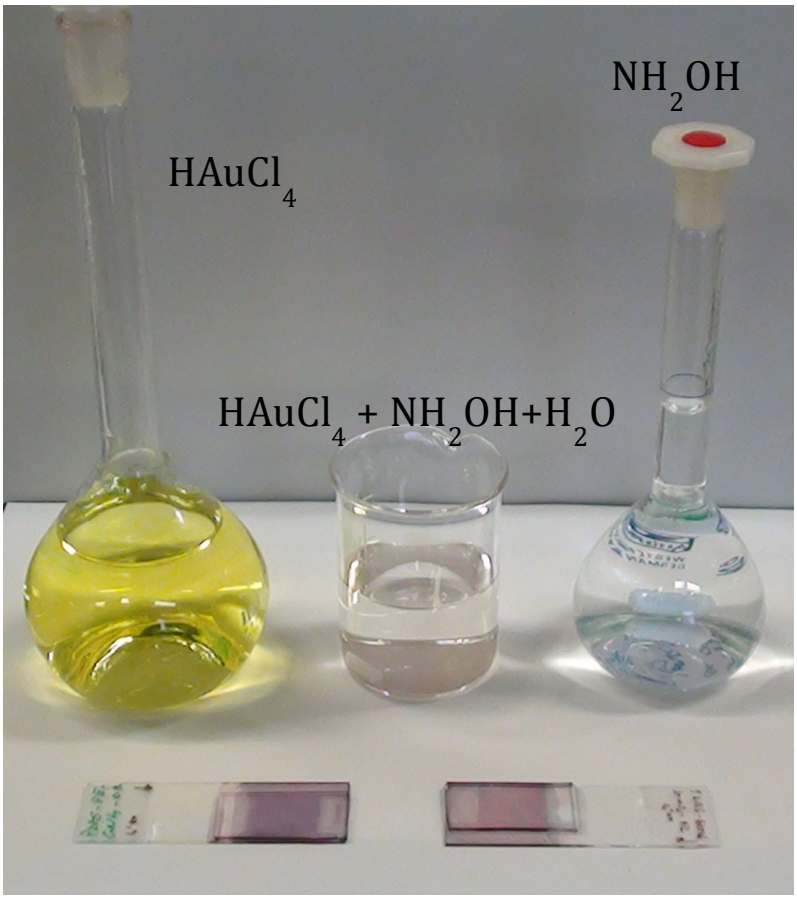

Figure 11. Chemical substances utilized in the growth process and obtained PDMS samples coated with grown GNPs.

II.5 Reference

1. P. G. DE GENNES and J. PROST, The physics of Liquid Crystal; Clarendon press – Oxford 1993
2. IAM-CHOON KHOO, Liquid Crystals second edition, WILEY-INTERSCIENCE A JOHN WILEY & SONS, INC., PUBLICATION**,** ISBN 978-0-471-75153-3
3. R. Caputo, L. De Sio, A.Veltri, C. Umeton, A.V. Sukhov, *Optics Letters,* 2004, Vol. 29 No.11 1261-1263
4. R.Caputo et alt., J. Opt A: Pure Appl. Opt. 11 (2009) 024017
5. L. De Sio, S. Ferjani, G. Strangi, C. Umeton and R.Bartolino, *Soft Matter* , 2011, **7**, 3739-3743
6. J.E. Gordon, Strutture sotto sforzo, Zanichelli editore, Bologna 1991
7. S. Rosati, Fisica generale, Casa editrice ambrosiana, Milano 1994
8. Fainman, Y., Lee, L. P., Psaltis, D., & Yang, C. (2010). *Optofluidics: Fundamental, Devices, and Application*. McGraw-Hill
9. F. Schneider, Jan Draheim, Robert Kamberger, Ulrike Wallrabe, Sensor and Actuators A 151 (2009) 95-99
10. Turkevich, J.; Stevenson, P. C.; Hillier, J. *Discuss. Faraday Soc.* **1951**, *11*, 55; Enu¨stu¨n, B. V.
11. Turkevich, J. *J. Am. Chem. Soc.* **1963**, *85*, 3317.
12. Frens, G. *Nat. Phys. Sci.* **1973**, *20*, 241.
13. J. Kimling, M. Maier, B. Okenve, V. Kotaidis, H. Ballot, and A. Plech; *J. Phys. Chem. B* **2006,** *110,* 15700-15707
14. Kenneth R. Brown and Michael J. Natan, *Langmuir* 1998, *14*, 726-728
15. Kenneth R. Brown, Daniel G. Walter and Michael J. Natan, *Chem. Mater.* 2000, *12,* 306-313

16. Kenneth R. Brown, L. Andrew Lyon, Audrey P. Fox, Brian D. Reiss and Michael J. Natan, *Chem. Mater.* 2000, *12,* 314-323

17. Dominik Enders, Tadaaki Nagao, Annemarie Pucci, Tomonobu Nakayama and Masakazu Aono, *Phys. Chem. Chem. Phys, 2011,* 13, 4935-4941.

III Active plasmonics driven by Cholesteric liquid crystal

Introduction

In this chapter, I illustrate how it is possible to obtain an active plasmonics system by utilizing a rigid and micro-periodic Policryps grating structure which has been infiltrated, by capillarity, with a mixture of cholesteric liquid crystal and GNPs. This mixture occupies the empty channels obtained by removing the original nematic LC material that was present between the polymer walls of the structure. The fabricated system has been operated by applying an external electric field or by modifying its temperature During the application of these external stimula, the spectral behaviour has been investigated in the UV-VIS range for two different polarization directions of the impinging probe light. It is worth noting that, during the infiltration process, a self-arrangement of the GNPs with the cholesteric phase takes place and realizes a new hybrid soft/hard matter: SEM imaging confirms a regular organization of the mixture along the grating. Correlation between the optical response and external perturbations (electric field, temperature variation) gives an outstanding example of broadband tuning of an “active” plasmon resonance. In this experiment, has been possible to exploit properties of reconfigurable soft materials to drive the resonance properties of noble metal nanoparticles, using an approach that put a bridge between soft matter and plasmonics.

III.1 Top-down and bottom-up approaches

One of the main goals of Nanotechnology is to manipulate matter on an atomic and/or molecular scale to fabricate functional materials with nanoscale features (the so called nanomaterials)[1]. Several approaches are exploited for realizing these materials but, very often, pros and cons of each of them seem to be almost balanced, and the right choice can be hardly taken. When using a "top-down" approach, matter is object of external actions that modify its structural properties; interference holography[2] or e-beam lithography[3] are examples of such an approach. In one case, large structures can be realized, but their resolution is limited by the wavelength of the writing radiation. In the other case, the electron beam can produce very resolute details, but the procedure is particularly cumbersome and time expensive so that the useful area of the obtained structure has to be, necessarily, very limited. When dealing with a "bottom-up" approach, functional nanostructures are organized by using a molecule-by-molecule arrangement: atoms and/or molecules self-assemble into a particular structure due to their peculiar properties.

III.2 Nanoparticles

In the last years, metallic nanoparticles (NPs) have been used as building blocks for realizing a new generation of nanomaterials with peculiar, unusual, optical properties. In particular, Gold and Silver NPs show plasmonic resonances when excited by a suitable electromagnetic radiation in the visible portion of the spectrum. Moreover, being these NPs well compatible with biological systems, proteins binding, oligonucleotides and other biologically relevant systems[4], their use can be crucial for the investigation of biological systems and in-vivo analysis[5]. Thus, it might be quite advantageous to move the particle plasmon resonance to the near-infrared region, between 550 and 900 nm, where water

and hemoglobin absorption coefficients exhibit a minimum[6]. The spectral position of this kind of resonance can be modified by properly varying the size and shape of the utilized particles; this feature is very attractive for possible applications and several cases have been already explored[7].

III.3 Liquid crystal as a host for active plasmonics

Despite recent results in Plasmonics are quite promising, mainly samples with static properties have been realized up to now. An ambitious project is to combine metallic units with host materials whose dielectric properties can be tuned by means of an external control; indeed, a modification of the dielectric response of the host material may yield a tuning action of the plasmon resonance frequency. To this end, Liquid Crystals (LCs) are an outstanding example of active dielectric medium: they combine self-organizing properties with fluidity, and can fulfill conditions imposed from outside, being quite responsive to a wide variety of external stimuli. In fact, LCs are made by anisotropic molecules possessing long range orientational order (see chapter II), a very broadband (0.4 μm–12 μm, in light wavelength) range of birefringence and transparency, and a high susceptibility to DC, AC and optical fields. Thanks to these properties, LCs have been widely used for realizing a voltage-induced shift of the selective absorptions of surface and localized plasmon resonances[8], all-optical plasmonic switch[9], to enhance[10] and for modeling[11] the electro-optical properties of LCs containing NPs, for large spectral tunability of metallic arrays layered with LCs[12,13] and for active modulation of nanorod plasmons[14]; at the same time, LCs can be exploited as a “host-fluid” for dissolving colloidal noble nanoparticles[15]. However, a drawback is represented by the fact that, in general, LCs require chemical and /or mechanical treatments to be aligned. In addition, the order

degree of the LC material is, in general, destabilized by the inclusion of nanoparticles and therefore their concentration in the host LC must be limited to few percents[16,17].

III.4 POLICRYPS as a template for plasmonic systems

Recently, we have reported on the realization of a periodic soft-composite structure, with a wide range of photonic applications, which might represent a solution to the previously illustrated drawbacks[18]. By a microfluidic etching of a composite micro/nano grating, made of polymer slices alternated to films of well oriented LC (POLICRYPS)[19], we realize a polymeric platform that is able to align and microconfine a large variety of LC materials, without the need of any chemical and/or mechanical treatment. In the following, we show that the same platform can be utilized for efficiently aligning Cholesteric Liquid Crystals (CLC) doped with Gold nanoparticles, as well.

III. 5 Experimental section

In order to obtain a homogeneous mixture of metallic nanoparticles (NPs) and CLC, we have used the Harima Gold nanopaste NPG-J (from Harima Chemicals, Inc., generally used for other aims like ink-jet printing and laser sintering), and the BL095 CLC by Merck (helix pitch ~ 400 nm). Harima nanopaste NPG-J contains 55%wt of Au NPs, with an average diameter of about 10 nm and a plasmonic absorption peak in solvent (naphthen) at λ=525 nm.

The Au NPs have been mixed to the CLC in high concentration (about 20% wt) and then infiltrated, by capillarity, in the polymeric template. The best optical performances were exhibited by a grating of *L*~10 mm thickness and L~6 mm pitch. The sample was kept at a fixed high temperature (~ 90 °C) during the whole filling process, thus keeping the CLC in

the isotropic phase; then, by slowly (0.5 deg/min) cooling down the sample to room temperature, a self-organization process occurred, which induced the axes of CLC helices to be oriented almost parallel to the polymeric slices, in a Uniform Lying Helix (ULH) configuration[18].

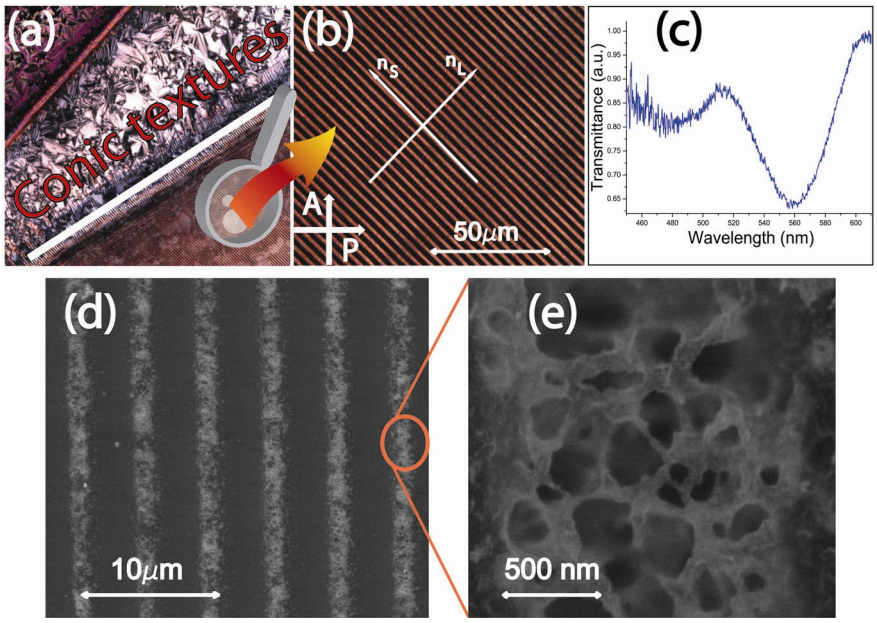

Figure 1: POM view of the polymeric template filled with CLC and Au NPs mixture at the edge of the grating area **(a)**.The high magnification of the CLC and Au NPs area aligned in ULH geometry is shown in **(b)** while its typical reflection notch is reported in **(c)**. EBSD view **(d)** and high magnification **(e)** of the polymeric template filled with CLC and Au NPs.

Fig. 1a shows a Polarized Optical Microscope (POM) micrograph of the sample at the edge of the photo-sculptured grating area; on the left, the photo puts into evidence the existence of a standard focal conic texture, induced by a random distribution of the helical axes. On the right, the polymeric structure induces a ULH geometry (Fig. 1b), as demonstrated by the presence of a selective reflection (stop band), typical of a short pitch CLC (Fig. 1c). Despite the quite high concentration of Au NPs, the high magnification in Fig. 1b indicates that the CLC exhibits a uniform alignment, with very well organized helices confined between polymeric slices. This is a clear indication that the CLC exhibits

good “host-fluidity” properties for the Au NPs; at the same time, its high degree of order indicates that the CLC phase is weakly perturbed by the presence of Au NPs. The obtained structure represents, in our opinion, the successful combination of a “top-down” approach (polymeric template fabrication) with a “bottom-up” one, represented by the self-organization of Au NPs in CLC helices; in this way the microscale meets the nanoscale. In order to study the effects produced by the presence of Au NPs inside the microstructure, we first tried to figure out their distribution within the CLC host by performing a Scanning Electron Microscope (SEM) and an Electron Back-Scattering Diffraction (EBSD) characterization of the sample. In particular, EBSD analysis is valuable to distinguish Gold from other materials, since the yield of backscattered electrons increases with the specimen atomic number (Z); in our case, the presence of Gold (Z=79) produces a high contrast with the polymer microstructure (a thiol based system with Z~18). As shown in the EBSD view of Fig. 1c, the bright stripes confirm the presence of Au along the microchannels only, while in the high magnification (Fig. 1d), we can notice, that CLC branches are literally “wrapped” by densely packed Au particles. Considering the size of involved NPs (~10nm), the SEM resolution is not able to show their morphological details.

III.5.1 Active plasmonics: tunability by applied electric field

In order to check the influence of Au NPs on the optical properties of the whole structure, we have investigated its spectral response by probing the sample with linearly polarized white light (wavelengths in the range 350-1000nm) at normal incidence; obtained results are reported in Fig. 2.

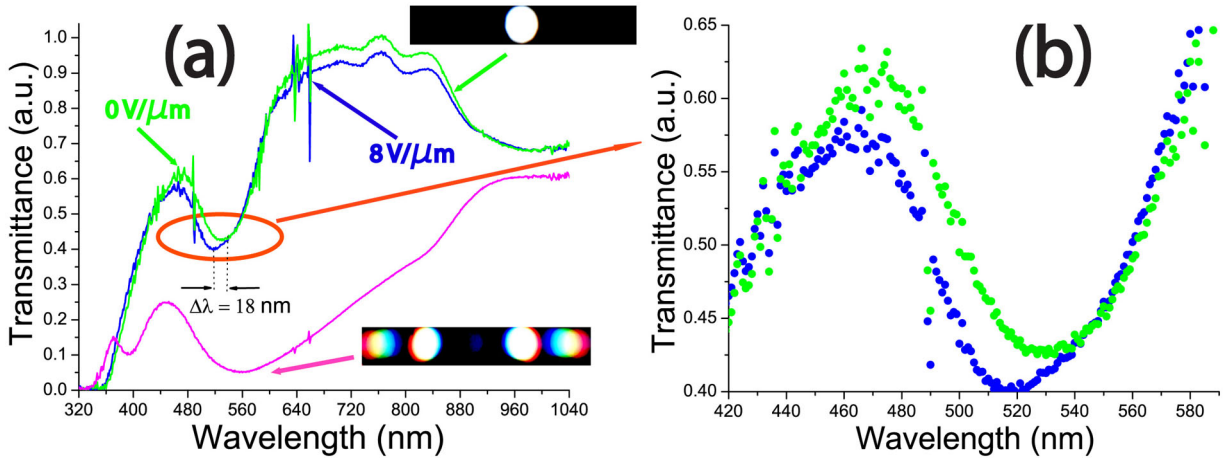

Figure 2: Spectral response of the sample for two values of the external electric field **(a)** and its higher magnification detail **(b)**.

It is evident that p-polarized light is strongly diffracted and its transmission is almost suppressed (diffraction pattern in the lower part of Fig. 2a and magenta curve respectively). On the other hand, s-polarized light is highly transmitted in almost the whole analyzed range (diffraction pattern in the upper part of Fig. 2a and green curve respectively). This behavior has already been observed in past with a similar structure[20] and can be easily explained by supposing that CLC helices lay, in average, along the channels of the template structure. It is reasonable to assume, therefore, that two different effective refractive indices exist: n_L (whose value can be estimated to be ~1.64), quite different from the polymeric refractive index n_p (~1.54), which is experienced by light whose electric field is perpendicular to the channels (p-wave), and n_S whose value can be estimated to be ~1.56 ~n_p, for light whose electric field is parallel to them (s-wave). Above rough estimation of n_S and n_L have been made by calculating two different averages of differently weighted ordinary and extraordinary refractive indices (n_o and n_e) of the CLC. Due to the alternation of n_L and n_p indices, the grating structure is therefore experienced only by the p-wave. Incidentally, the noticeable difference between n_L and n_S values is

confirmed by the pronounced birefringence shown by the sample (Fig. 1b, picture taken between crossed polarizers).

In the green curve of Fig. 2a, a pronounced absorption peak at λ=532 nm, with an extinction coefficient of 0.2 can be observed. This peak cannot be attributed to any diffractive mechanism because the structure appears optically homogenous ($n_S \sim n_p$) to the incoming s-wave. Both the spectral position and the narrow width of the measured peak suggest, instead, that it is due to the presence of Au NPs dispersed in the CLC host and, more precisely, to their localized plasmon resonance. This hypothesis is supported by similar results reported in literature [8], and observed in different systems where Au NPs are also involved[21]. Even if physically remarkable, this result is not outstanding in itself. It is quite interesting, on the contrary, the circumstance that the plasmonic response of such a composite nanomaterial is also tunable. This has been demonstrated by applying an external electric field (8 V/μm, frequency 1 Khz, square wave) across the cell, perpendicularly to the helix axes. This field induces an in-plane tilt of the optical axis of the CLC (aligned in ULH texture), with a consequent variation of the n_S refractive index of the CLC, experienced by s-waves. This index variation is directly related to the tuning of the plasmon resonance frequency. Indeed, the optical properties of spherical particle dispersions can be predicted by the Mie theory[22] through the expression of the extinction cross section.

$$\sigma_{ext}(\omega) = 9\frac{\omega}{c}\varepsilon_m^{3/2} V_0 \frac{\varepsilon_2(\omega)}{\left[\varepsilon_1(\omega) + 2\varepsilon_m\right]^2 + \varepsilon_2(\omega)^2} \qquad \text{(III.1)}$$

where $V_0 = (4\pi/3)R^3$ is the nanoparticles voleme, R being its radius, ω is the angular frequency of the exciting radiation, ε_m is the dielectric function of the medium surrounding the metallic nanoparticles, and ε_1 and ε_2 are the real and imaginary parts of the dielectric function of the metallic nanoparticles respectively. Based on this theory, for small and isolated metal particles, the spectral position of the plasmonic absorption peak depends on

the refractive index of the surrounding medium, according to the condition that minimizes the denominator of equation (III.1):

$$\varepsilon_1(\omega) = -2\,\varepsilon_m \qquad \text{(III.2)}$$

A modification of the dielectric behavior of the host material corresponds, therefore, to a tuning action of the Plasmon resonance frequency. In our case, when applying the external electric field, the impinging probe light experiences a decreasing value of the refractive index of the CLC (from n_S to about n_o; typically from 1.56 to 1.5). Following equation (III.2), the resonance condition is fulfilled for higher (negative) values of $\varepsilon_1(\omega)$. It is well known that, in the visible range, the real part of the electric permittivity of Gold nanoparticles increases with frequency[23]; therefore, fulfillment of equation (III.22) takes place for higher values of ω. This yields a blue shift of the plasmonic absorption peak. This hypothesis is confirmed by results shown in Fig. 2b (higher magnification of the highlighted region of Fig. 2a): the absorption peak is blue shifted from λ=532 nm (green curve Fig. 2b) to λ= 514 nm (blue curve, Fig. 2b).

III.5.2 Active Plasmonics: tunability by change of temperature

An additional demonstration of the tunability of the plasmonic response of our composite structure has been obtained by varying the temperature of the sample; results are reported in Fig. 3.

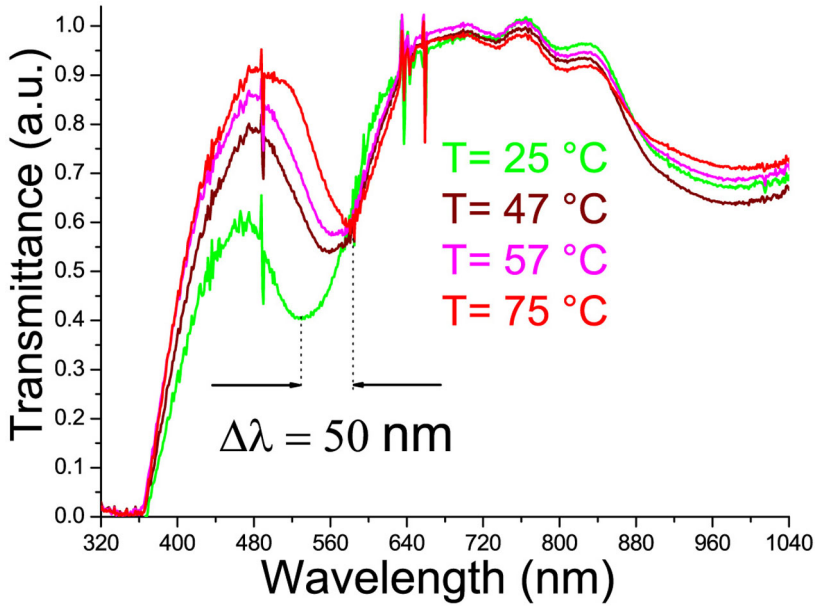

Figure 3: Spectral response of the sample versus its temperature.

By means of a miniature oven (CaLCTec S.r.l.), it was possible to vary the sample temperature from 25 °C up to 75 °C; a red-shift of the plasmonic absorption peak was observed in the range from 532 nm to 582 nm. It is well known[24] that the pitch *p* of chiral liquid crystals elongates with temperature; if we assume that the CLC helices are wrapped by Au NPs, the consequence of this elongation is an increase of the inter-distance between neighboring metal NPs. It has been demonstrated that the plasmon response of NP arrays depends on particle size and density[25,26]. Results show that, for densely packed metal NPs, the absorption peak is quite broad and is centered in the blue-green range; this peak slightly reduces its width and shifts to the red in case of well separated NPs. Indeed, as observed by Kinnan and Chumanov[27], when NP aggregates are considered, whose

size is comparable with the wavelength of the incoming radiation, different areas of the aggregates experience different phases of the incident radiation; thus, higher multipolar modes (quadrupolar, octupolar and even hexadecapolar) have to be taken into account. Given that the excitation frequency of these higher modes is larger than the dipolar one, a macroscopic broadening of the plasmon peak occurs which has its center in the blue region of the electromagnetic spectrum. On the contrary, single, small-sized, NPs, when hit by the incoming radiation, experience the same phase of the electromagnetic wave on their whole area; in this condition, NPs behave as simple dipoles: the plasmonic peak width is quite narrow and, depending on the particle size, the peak is centered in the green-red part of the electromagnetic spectrum. Based on the above considerations, the temperature dependent shift of the plasmonic resonance observed in our sample can be therefore explained in terms of a temperature induced passage from densely packed to mono-dispersed Au NPs.

III.6 Conclusions

In conclusion, we have reported on the realization and characterization of a soft-matter periodic structure containing a composite mixture of CLC and Au NPs. For them, the CLC material acts as a “host fluid” whose refractive index can be varied in a broad range, by utilizing both external electric fields and temperature variations. This has a strong influence on the position of the plasmonic absorption peak of NPs which exhibits, consequently, a broad tenability, thus enabling us the possibility to exploit the concept of “active plasmonics”. As a proof of concept, this is the first step towards the realization of a new generation of nanostructured materials with tunable optical properties.

III.7 References

1. R. F. Service, *Science* **2001**, 294, 2442.
2. L. Z. Cai, X. L. Yang, Y. R. Wang, *Opt. Lett.* **2002**, 27, 900.
3. M. A. McCord, M. J. Rooks, Handbook of Microlithography, Micromachining and Microfabrication. Volume 1: Microlithography. In *Electron Beam Lithography*, Rai-Choudhury, P. Editor; SPIE Press **2000,** 128.
4. T. J. Cho, R. A. Zangmeister, R. I. Maccuspie, A. K. Patri, V.A. Hackley, *Chem Mater.* **2011**, 23, 2665.
5. J.N. Anker, W.P. Hall, O. Lyandres, N.C. Shah; J. Zhao, R.P. Van Duyne, *Nat. Mater.* **2008**, 7, 442.
6. C. Sonnichsen, A. P. Alivisatos, *Nano Lett*. **2005**, 5, 301.
7. L. M. Liz-Marzan, *Mater. Today* **2004**, 7, 26.
8. P.A. Kossyrev, A. Yin, S.G. Cloutier, D.A. Cardimona, D. Huang, P.M. Alsing, J.M. Xu, *Nano Lett.* **2005**, 5, 1978.
9. V. K. S. Hsiao, Y. B. Zheng, B. K. Juluri, T. J.Huang, *Ad. Mat*. **2008,** 20, 3528.
10. S. Khatua, P. Manna, W. S. Chang, A. Tcherniak, E. Friedlander, E. R. Zubarev, S. Link, *J. Phys. Chem. C* **2010**, 114, 7251.
11. M. Dridi, A. Vial, *J. Phys. Chem. C* **2010**, 114, 9541.
12. Y. J. Liu, Q. Hao, J. S. T. Smalley, J. Liou, I. C. Khoo, T. J. Huang, *App. Phys. Lett.* **2010**, 97, 091101.
13. J. Li, Y. Ma, Y. Gu,I. C. Khoo, Q. Gong, *App. Phys. Lett.* **2011**, 98, 213101.
14. S. Khatua, W.S. Chang, P. Swanglap, J. Olson, S. Link, *Nano Lett*. **2011**, 11, 3797.
15. R. Pratibha, W. Park, I. Smalyukh, *J. App. Phys.* **2010**, 107, 063511.
16. T. Hegmann, H. Qi, V.M. Marx, *J. In. Org. Pol. Mat.* **2007**, 17, 483.
17. M. Mitov, C. Portet, C. Bourgerette, E. Snoeck, M. Verelst, *Nat. Mater.* **2002**, 1, 229.
18. L. De Sio, S. Ferjani, G. Strangi, C. Umeton; R. Bartolino, *Soft Matter* **2011**, 7, 3739.

19. R. Caputo, A.V. Sukhov, A. Veltri, C. Umeton, *J. Opt. Soc. of Am. B* **2004**, 21, 1939.
20. G. Strangi, V. Barna, R. Caputo, A. de Luca, C. Versace, N. Scaramuzza, C. Umeton and R. Bartolino, *Phys. Rev. Lett*. **2005**, 94, 063903.
21. S. Link and M.A. El-SayedJ. Phys. Chem. B **1999**, 103, 4212.
22. G. Mie, *Ann. Phys* **1908**, 25, 377.
23. P. B. Johnson, R. W. Christy, *Phys. Rev. B* **1972**, 6, 4370.
24. P. G. de Gennes, J. Prost, The Physics of Liquid Crystals, 2nd ed., Clarendon Press, Oxford, **1993**.
25. F. Tam,; G. P. Goodrich, B. R. Johnson, N. J. Halas, *Nano Lett.* **2007,** 7, 496.
26. U. Kreibig, M. Vollmer, Optical Properties of Metal Clusters, Springer-Verlag, Berlin, **1996**.
27. M. K. Kinnan,; G. Chumanov, *J. Phys. Chem. C* **2010**, 114, 7496.

IV Active Plasmonics driven by Mechanical Strain

IV.1 Introduction

The bright colours due to the interaction of light with noble metals, (mainly gold and silver) has been exploited in the past to increase the value of objects, as the famous Licurgus cup, or of monumental buildings, as Cathedrals with their stained glasses. In both examples, characteristic well-defined colours are the response of nano-size fragments of noble metals, (in colloidal phase) under the stimulus of light. The physical phenomenon at the basis of this behaviour is the localized surface plasmon resonance (chap. I) that nanoparticles show, as a peak of absorbance at a well-defined wavelength, when illuminated by white light. The resonance condition depends on the medium surrounding the nanoparticles and on the relative distance between them: when metal nanoparticles are very close, near-field coupling leads to concentrated and highly localized electric fields. This phenomenon is at the origin of many applications, for example in sensing [1-3] and in the design of metamaterials [4].

Since, coupling and optical properties of the sample sensitively depend on the distance between nanoparticles[5,6], this has to be controlled with nanometer precision, in order to obtain the designed optical properties of a given sample. A prototypical example of coupled plasmonic system is represented by two gold nanoparticles, a dimer, brought together at a gap (border-to-border) as close as half of their diameter or less[7]. In this case, if the impinging light is polarized along the dimer axis, a shift of the original plasmon resonance (e.g. the resonance wavelength due to isolated nanoparticles) can be observed in the extinction spectrum, which depends exponentially on the distance between the coupled particles[8,9]. Thus, interesting opportunities would emerge from the possibility to control at the nanometer scale the distance between the coupled plasmonic particles.

IV.2 Experiment description

In the following, we show that the realization of this control is as simple as pulling an elastic tape covered by gold nanoparticles. In this case, the distance between them is mechanically controlled by stretching the elastic tape in one direction, which leads to a compression in the direction perpendicular to the stretching. The result is a colour change of the sample due to a change in the interaction of neighbouring nanoparticles. At the nanoscale, this means that the electric field of interaction between the particles can be manipulated by using a mechanical strain.

The basic idea is given in Figure 1a, while the real system we realized is shown in Figure 1b, both in its relaxed and stretched states: upon stretching, the colour changes from magenta to blue-violet.

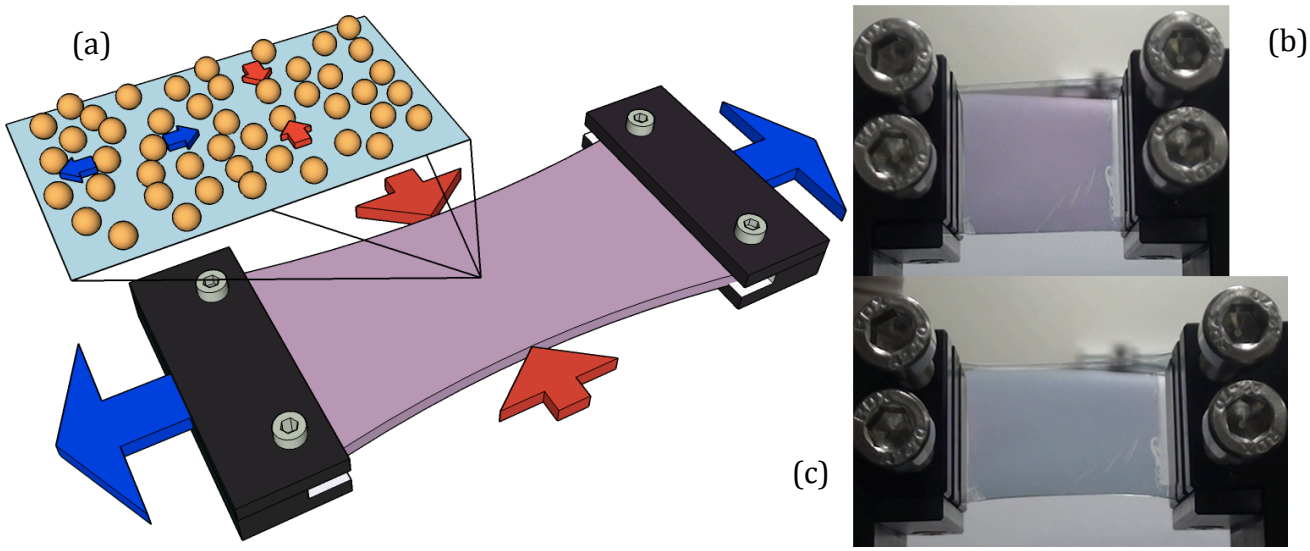

Figure 1. **(a)** Sketch of the experimental setup. By stretching a PDMS sample coated with a single layer of gold nanoparticles the average distance between them becomes larger in the stretching direction and shorter in the perpendicular one. Stretching of the sample is accompanied by a remarkable change of colour from purple-red **(b)** to blue-violet **(c).** Images were acquired with a polarizer, mounted to a camera, with direction of polarization perpendicular to the applied strain.

IV.3 Sample preparation and growing process

Samples have been prepared by using self-assembly techniques from nanochemistry, and they have been fabricated in multiple steps. First the PDMS elastomeric template (Fig. 2) was obtained by mixing in a baker elastomeric and curing agent in 1:10 weight ratio. The mixture was then poured in a glass petri dish. Afterwards, the petri dish was baked in the oven at 80°C for one hour. After the baking step, the hardened PDMS substrate was peeled off from the petri dish and cut into pieces with a size of (26 mm x 16.6 mm x 1.2 mm).

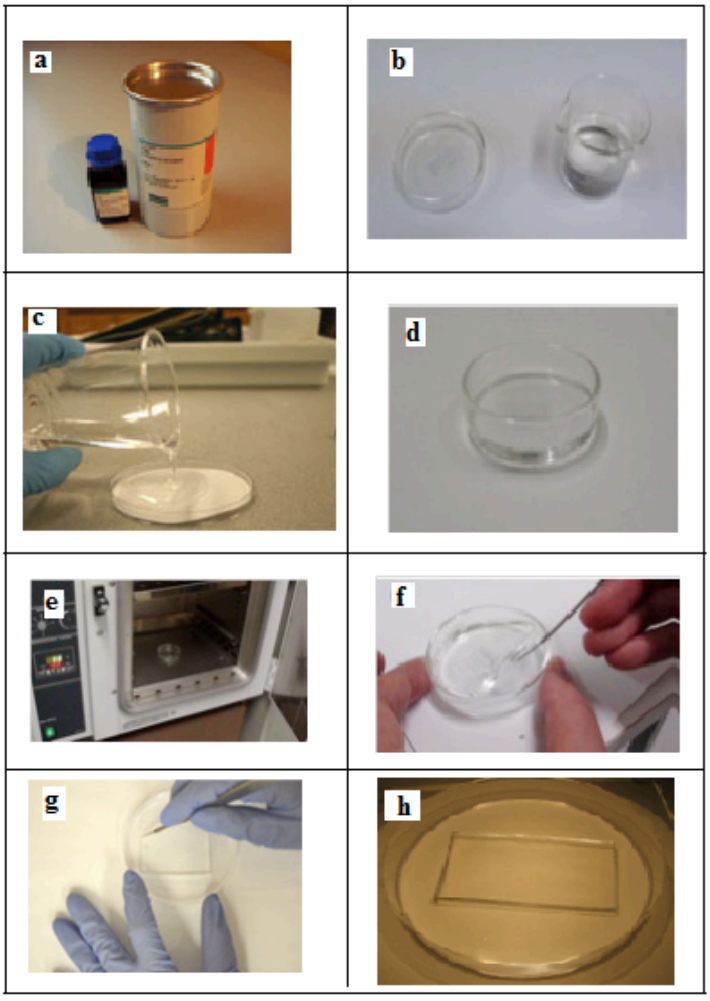

Figure 2. Template preparation**: (a)** PDMS Sylgard components: curing agent (left) and elastomer (right) **(b)** liquid mixture preparation **(c)** liquid mixture in petri-dish **(d)** degassing phase **(e)** curing phase in a oven **(f)** peeling off **(g)** cutting of template **(h)** template ready to be covered with gold nanoparticles**.**

Gold nanoparticles were prepared as already described in paragraph II.4.1.

A monolayer of GNPs was prepared; the obtained GNPs have been as seeds to be grown, at a later stage, to the desired size. In order to prepare this monolayer the PDMS template was first rinsed with water and ethanol and then dried up under a stream of air. Then, it was exposed to a plasma air treatment (806 mTorr with a constant flux of air of 31.94 mL/min, 90 sec, 7.2 Watt), which leaded to the oxidation of the surface. Immediately after this step, the template was dipped in a solution of Milli Q-water and 1% of 3-Aminopropyltriethoxysilane (from Sigma Aldrich) for 30 min. The template was then rinsed very well with Milli Q-water and dried with a stream of air. After that, the functionalized template was dipped in the GNPs solution for 2.5 hours. After the removal from the GNPs solution, the sample was rinsed and dried up as before.

The growing processes of GNPs seeds attached on the PDMS[10-13] has been realized by dipping the sample in Au^{3+}/NH_2OH solution (0.3 mM $HAuCl_4$,Alfa Aesar), 0.4 mM NH_2OH (Sigma- Aldrich)) at room temperature. Each growth cycle lasted 2 minutes. After each step the sample was washed and dried up to remove excess materials. In Fig. 3 we show a sample with the monolayer with GNPs not grown (a) and after 12 cycles of growth (b). We can note the change of colour due to the growth process.

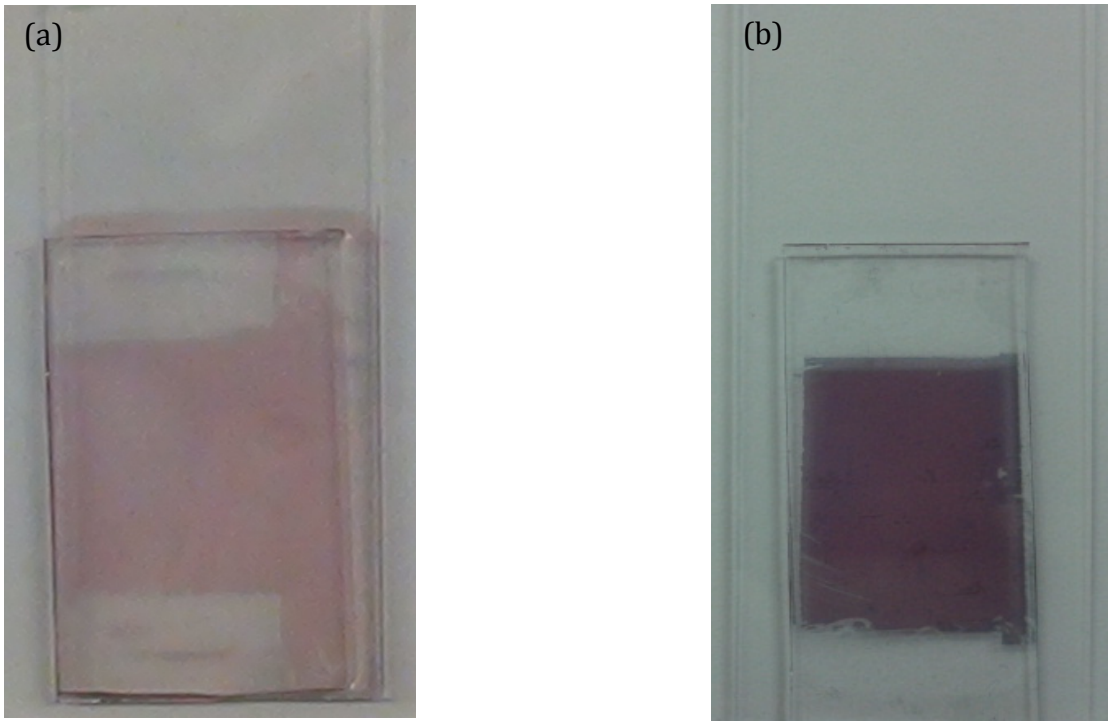

Figure 3. (a) Monolayer of gold nanoparticles not grown; **(b)** Same sample with the monolayer of gold nanoparticles after 12 cycles of growth.

SEM images acquired successively on stripes cut from the sample reported in Figure 3, are shown in Figure 4:

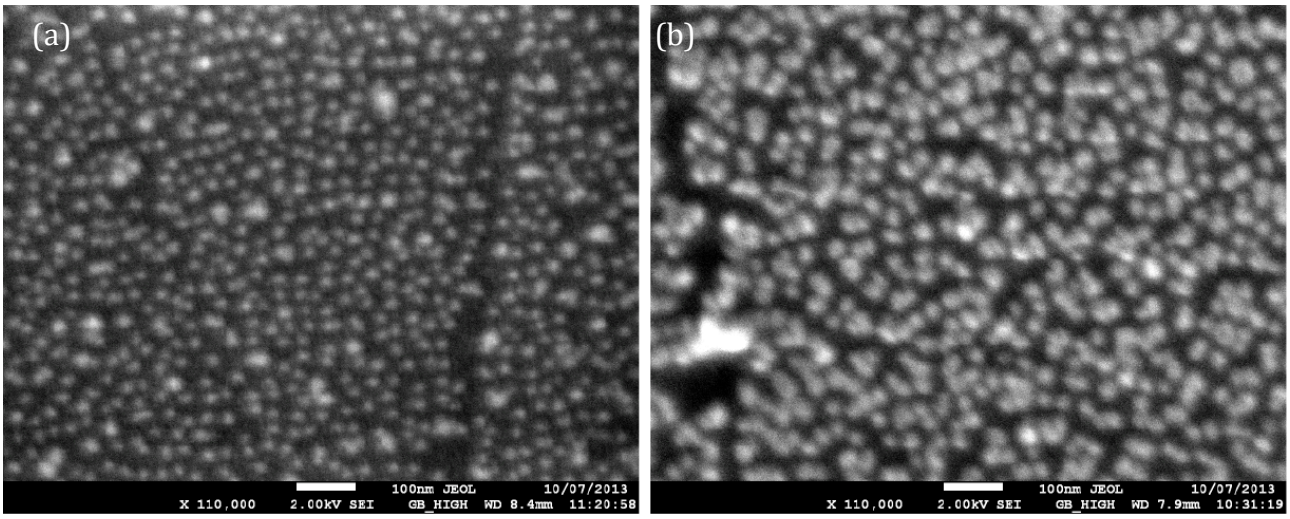

Figure 4: SEM images of sample with **(a)** monolayer of gold nanoparticles ungrown(Figure 3. (a)) and **(b)** the same monolayer after 12 cycles of growing (Figure 3. (b)).

Nanoparticles sizes have been measured from SEM images and average diameters are, 23 nm for not grown particles and 32nm for particles after 12 cycles of growth.

IV.4 Stretching apparatus and extinction spectra acquisition

For the acquisition of spectra at rest and under stress, a platform was built with two mobile clamps controlled and moved apart symmetrically by two-micrometer screws with resolution of 700 microns. The fabricated platform was positioned in the Varian V-670 UV/VIS/NIR Spectrophotometer (Fig. 4.a) used for all extinction spectroscopy experiments. The sample was mounted between tweezers (Fig.4.b) and positioned perpendicularly to the probe beam. For every step of stretching (relaxing), the corresponding spectrum was acquired. Measurements were acquired with both un-polarized and polarized light. For polarized light experiments, two polarizers were mounted in correspondence of the reference and the sample beam outputs within the spectrophotometer.

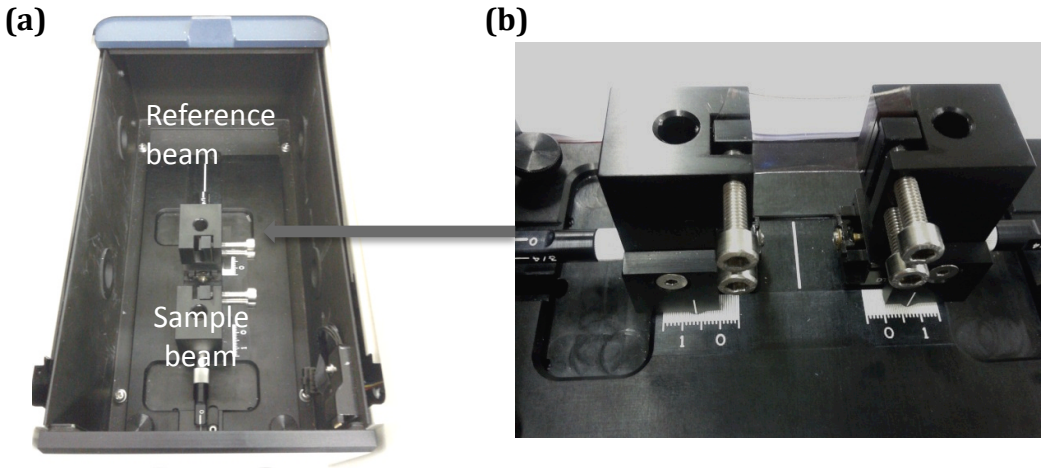

Figure 4. Experimental set-up, **(a)** Varian V-670 UV/VIS/NIR Spectrophotometer **(b)** Stretching platform home-built with two mobile clamps moved apart from two-micrometre screwes

In order to obtain the extinction exclusively due to coupled nanoparticles (excluding any contribution from the flexible substrate), PDMS samples identical to the ones used for the experiments (same size and thickness), but without nanoparticles, were analyzed under identical stretching conditions. The extinction spectra of the PDMS substrates have been then subtracted from the spectra of the samples with nanoparticles. This procedure has been repeated for all the analysed samples.

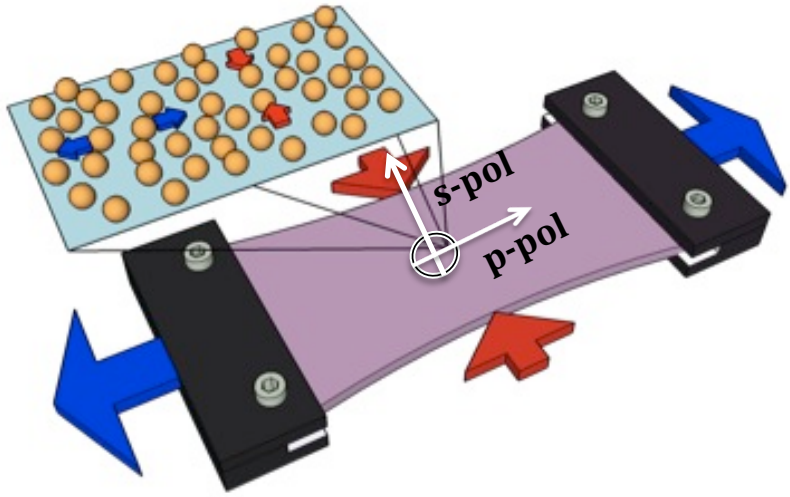

Figure 5. Spectra acquisitions on stretched sample**:** in the diagram it is showed a representation of the sample stretched and shined with a polarized beam orthogonally to surface. The two polarizations (white arrows), are longitudinal (p-pol) and transversal (s-pol) to direction of stretching (blue arrows).

IV.6 Optical characterization.

The first performed experiment has been conducted by acquiring the spectra under stretching of the same sample but after different cycles of growth of the particles with the probe beam polarized along and perpendicularly to the direction of stretching. In figure 6 are shown the spectra acquired by analysing the sample with the not grown monolayer, while in fig. 7, there is the same characterization made on the sample with the monolayer grown 12 times.

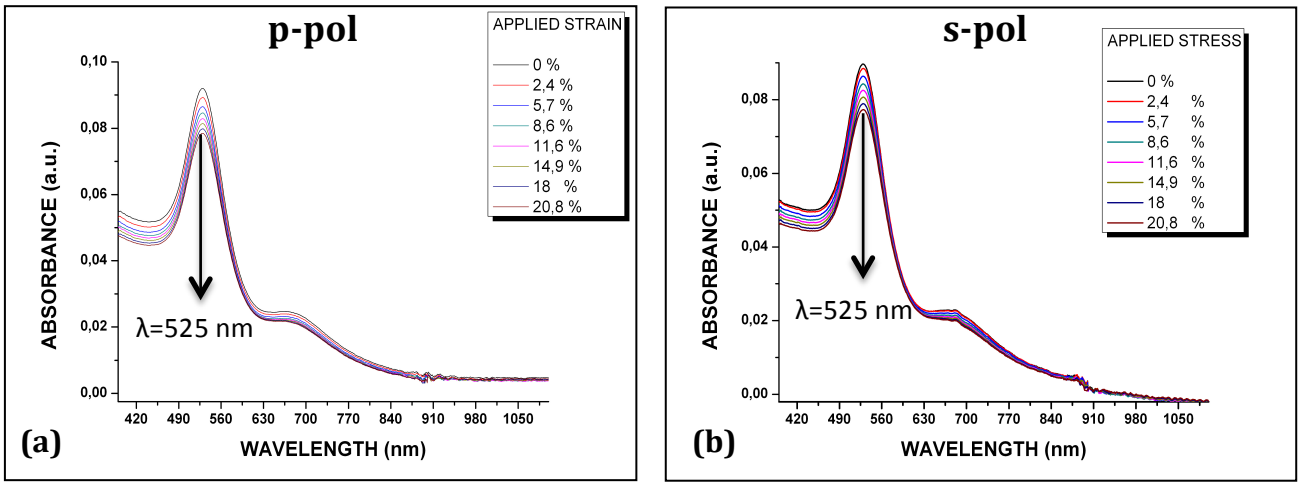

Figure 6. Spectra acquired by analysing the sample with the not grown monolayer under stretching with **(a)** p-polarized beam probe and **(b)** s-polarized beam probe.

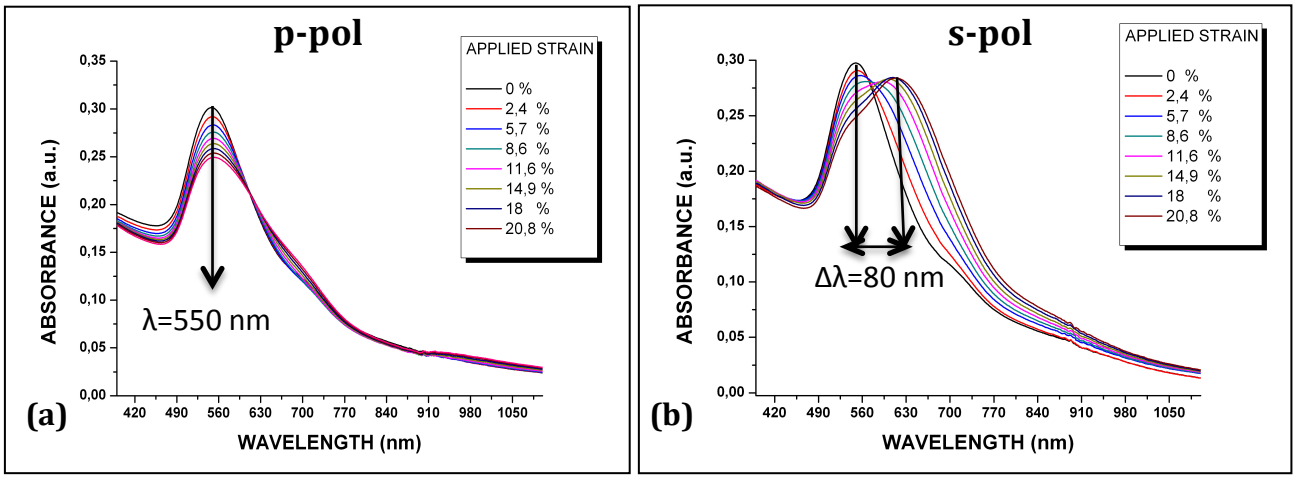

Figure 7. Spectra acquired by analysing the sample with the monolayer grown 12 times under stretching with **(a)** p-polarized beam probe and **(b)** s-polarized beam probe. In (b), the overall plasmon resonance red-shift covered by the spectra is of about 80nm, ranging from 550 nm to 630 nm.

From the comparison of Fig. 6 and Fig. 7, it is clear that the processes of growth change the plasmonic response of the sample: there is an increasing of absorbance (from 0.1 to 0.3) with the sample at rest, and a broadening of the single curves: these two effects are mainly due to increasing of size of the gold nanoparticles. When stretching is applied to not grown particles (Fig. 6a,b) the effect is a decrease of the absorbance due to the

decrease of local density of nanoparticles: because of stretching, the area covered by nanoparticles increases but their number remains the same. The peaks position remains fixed at the same wavelength (525 nm). This means that gold nanoparticles are so far from each other that their near-fields are uncoupled.

When stretching is applied to the sample with grown nanoparticles, the behaviour is different if spectra are acquired with a p- or s-polarized probe beam: in the first case, Fig. 7a, we observe a decrease of the absorbance and a broadening of the curves, while peaks of resonance position remain constant at 550 nm, as in case of the sample at rest. This means that even if nanoparticles have increased their sizes, the effect of stretching is an increase of their inter-distances which still keeps them in an uncoupled condition.

S-polarized beam probe, impinging above the stretched monolayer grown 12 times, produces instead a dramatic effect on the plasmon resonance position: while stretching, the single-particle dipolar tends to decrease its absorbance value to the point that, at 20,8% of applied strain, it becomes just a shoulder of a second peak (appeared during stretching) which is red-shifted of about 80 nm with respect to the first one. In this stretching condition, This second peak shows the maximum value in correspondence of a wavelength of 630 nm and about the same absorbance value of the dipolar peak acquired with the sample at rest. This behaviour can be explained by taking into account the decrease of 10,4% of the inter-distance (center-to-center) between nanoparticles that takes place in the direction perpendicular to the applied stretching. This particles approach is related to due to the fact that the sample is stretched in elastic regime. In order to confirm this regime for our experiments, from the video taken during the experiment, we extracted the macroscopic values of compression and elongation that the sample underwent during the different stretching steps (post-processing by ImageJ software). The Poisson's coefficient value was then calculated from the fit of the graph (inset Fig. 8a) of compression vs applied strain. Within the experimental error, all obtained values up to a

stretching percentage of 20.8% (inset Fig. 8a) confirm a Poisson coefficient of about 0.5 (0.4996±0.0283). This result implies that, if the sample is stretched of 20.8%, perpendicularly is compressed of 10.4%, precisely by the half.

During the experiment, spectra have been acquired by first increasing and then releasing the applied strain. The optical behaviour observed in Fig. 8 is almost identical, (inset Fig.8b shows only a slight hysteresis) denoting that the changes induced in the sample are fully reversible. These spectra unequivocally show no agglomeration or clusterization between nanoparticles. Indeed, these phenomena would be irreversible[14,15] and related spectra would just show a broad resonance peak centered at a high wavelength without any reversibility[16].

This radical change of the plasmonic response, due to the decrease of the inter-distance between grown spherical gold nanoparticles anchored on the PDMS template, is only obtained by a compression action. This suggests that a much deeper physical phenomenon happens at the nanoscale. Most probably, when nanostructures approach each other, their plasmonic near-fields begin to couple. To proof this hypothesis, a possibility is to identify the observed behaviour in the picture of the plasmon ruler, already described in chapter I.

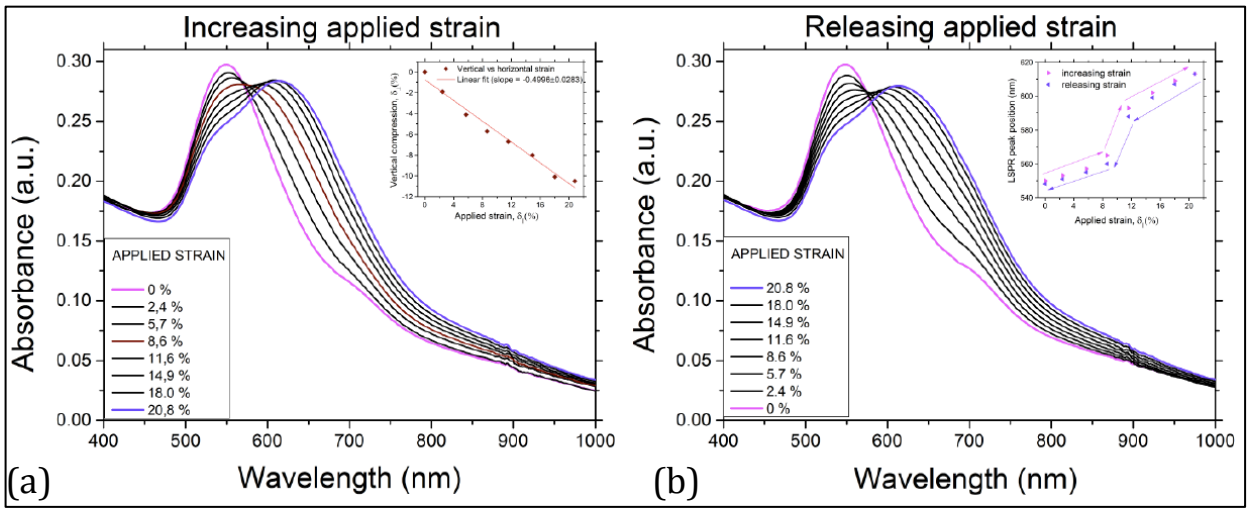

Figure 8. (a) Extinction spectra of the sample coated with gold nanoparticles (after twelve cycles of growth) acquired while increasing the applied strain from 0% to 20.8%. The sample has been irradiated with an s-polarized light. In the inset, the measurement of the percentage compression, which the sample undergoes in the direction perpendicular to the applied strain, is reported; a Poisson coefficient of about 0.5 is confirmed for the PDMS substrate. **(b)** Extinction spectra acquired by releasing the strain applied to the same sample from 20.8% to 0%. The inset shows the spectral position of the resonance peak maxima as a function of the applied strain, during a straining-releasing cycle. A slight hysteresis is observed.

It is noticeable that this anisotropic plasmonic behaviour comes out from an isotropic system of growth gold nanoparticles by only applying an elastic and unidirectional perturbation. Another way to underline this result is reported in Fig. 9a, b, where we show the absorbance spectra **(a)** at maximum stretching of 20.8%, and **(b)** at rest, acquired with an s-polarized probe after each cycle of growth.

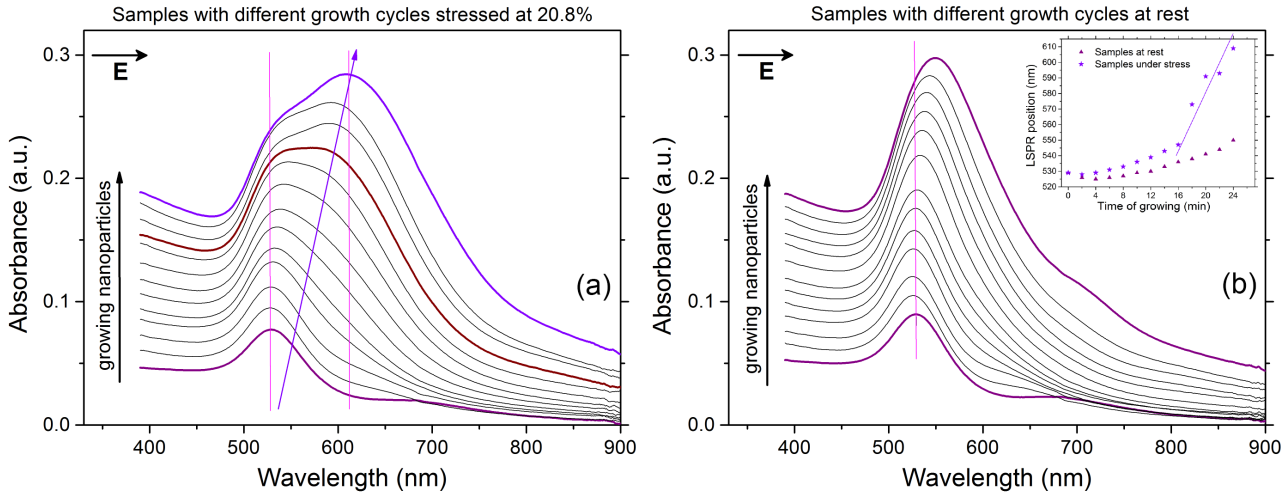

Figure 9. Extinction spectra of gold nanoparticle coated PDMS samples with different numbers of growth cycles of the particles, in case that (a) an applied strain of 20.8% is applied and (b) samples are at rest. Sample are irradiated with s-polarized light. In the inset, the plasmon peak position is plotted as a function of the number of growth cycles for samples at rest (triangles) and under stress (stars).

We can observe that with the sample at rest, the growth of particles leads to a moderate shift of the localized surface plasmon resonance (triangles in the inset of Fig 9 b). When a strain is applied, a moderate though larger shift is observed after few growth cycles (three to eight). However, after many cycles (nine to twelve) the stretching has a dramatic effect: in fact, particles in the relaxed state are so close that a slight change in their relative distance has a huge consequence on the coupling effect and hence on the resonance shift. This drastic change in the slope of the curve is, in our opinion, a qualitative confirmation that a plasmonic coupling effect takes place in the system.

IV. 6 Dependence of system Potential energy from polarizer beam configuration.

A way to interpret the anisotropic behaviour, illustrated in the last part of previous paragraph, is to consider the potential energy change of random dimers. In this section, we consider this argument by taking into account the presence of a strain parameter to the treatment made in I.3.4.

V.6.1 Potential energy variation of a dimer during the application of a mechanical strain.

As already written, the potential energy existing between two interacting dipoles put at distance **r** can be written as:

$$U = -\frac{\xi|\mu|^2}{4\pi\varepsilon_0 r^3} \qquad \text{(IV.1)}$$

where the factor $\xi=3\cos\theta_1\cos\theta_2-\cos\theta_{12}$ takes into account the relative orientation of the interacting dipoles between each other and with respect to the exciting field **E**, as sketched in Fig. 10

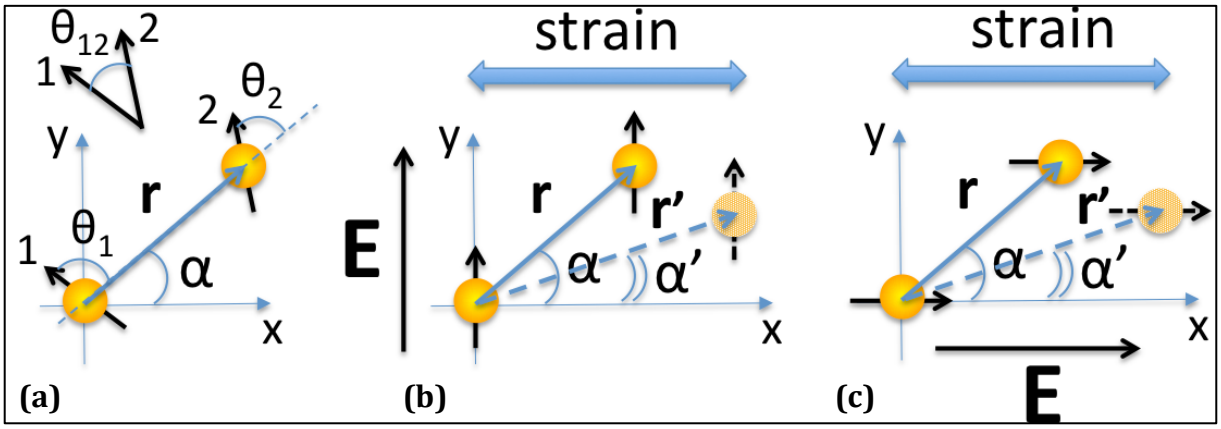

Figure 10. Sketch of coupled nanoparticles considered as interacting dipoles. (a) general situation of two interacting dipoles; (b) Excitation of a dimer with s-polarized light and geometrical configuration with and without applied strain; (c) Excitation of a dimer with p-polarized light and geometrical configuration with and without applied strain.

In more details, θ_1 and θ_2 are the angles respectively formed by dipole 1 and dipole 2 with **r** while θ_{12} is the angle they form with each other. If the relative position of the two interacting plasmonic particles is modified by the macroscopic strain applied to the PDMS substrate where they are immobilized, the energy variation ΔU related to the new configuration can be written as:

$$\Delta U = U'_{s,p} - U_{s,p} = -\left(\frac{\xi'_{s,p}|\mu|^2}{4\pi\varepsilon_0 r'^3} - \frac{\xi_{s,p}|\mu|^2}{4\pi\varepsilon_0 r^3}\right) \qquad \text{(IV.2)}$$

where $r'=r[(1+f)^2\cos^2\alpha+(1-0.5f)^2\sin^2\alpha]^{1/2}$ is the distance, after strain, between considered particles and α is the initial angle made by **r** with the x-axis (Figs. 10 b,c). In the

expression for r' it has been also considered that, for all applied strains (f=0%÷20.8%), the PDMS sample is in elastic regime (PDMS Poisson's ratio ≈ 0.5). As far as ξ values are considered, since dipoles 1 and 2 are induced by the exciting field **E**, they are oriented parallel to it, hence $\theta_1=\theta_2=\theta_{s,p}$ and $\theta_{12}=0$ while $\theta_s=\pi/2-\alpha$ for s-polarized field, **E||y** and $\theta_p=\alpha$ for p-polarized field **E⊥y**. As such, in our specific case, the polarization-dependent expressions for ξ are:

$$\xi_s = 3\cos^2\left(\pi/2 - \alpha\right) - 1 \quad ; \quad \xi_p = 3\cos^2\left(\alpha\right) - 1 \qquad \text{(IV.3)}$$

In Fig. 11a,b, Eq. IV.2 is plotted as a function of the angle α and for several values of the strain parameter f.

IV.6.2 Potential energy of the system and plasmonic shift

As for the dependence of the observed effects on the polarization of the impinging light, we underline once more that, quite surprisingly, our samples, which are amorphous and initially isotropic in the x-y plane, develop highly polarization-dependent optical properties after undergoing a stretching of about 20% only. In the following we suggest an interpretation of the red-shift of the plasmonic resonance wavelength based on potential energy arguments. The polarized illumination induces a dipole in each nanoparticle of the dimer; the latter can be represented, therefore, by two parallel dipoles, initially separated by a distance r (center-to-center), whose axis forms an angle a (Fig. 10) with the stretching direction (x). As such, the coupling between nanoparticles can be qualitatively figured out in the framework of the exciton-coupling model[11], originally developed to explain shifts observed in the spectra of dimerized organic molecules. The interaction energy U between the two particles of a dimer changes upon stretching and it is a function of the angle a

between the dimer axis and the stretching direction x. The energy variation ΔU (Eq. IV.2) between two stretched states can be both positive or negative and, as demonstrated in [8], corresponding to a blue or a red-shift of the plasmon band respectively. In Fig. 11a,b, ΔU is plotted as a function of the angle α and for several values of the strain parameter f. As a general feature, both graphs show that, for a given polarization of the exciting light, the energy variation strongly depends on the angular interval which α belongs to. In particular, the plot in Fig. 11a indicates that, for a polarization perpendicular to the stretching direction, $\Delta U_s<0$ for $0°<\alpha<25°$ and $70°<\alpha<90°$, while $\Delta U_s>0$ for $25°<\alpha<70°$. For $\Delta U_s<0$ ($\Delta U_s>0$) a red-shift (blue-shift) of the plasmon band is expected. Since our hypothesis is that samples at rest contain only monodispersed, non-interacting, particles put at an average distance r, above considerations on ΔU_s and related shifts can be applied only to those dimers whose interparticle distance r decreases upon stretching. Fig. 11c reveals that, upon stretching, this distance decreases and therefore a coupling effect takes place only for large angles ($60°<\alpha<90°$). Due to the effect of the angle a on distance and interaction energy, a pronounced dependence of the plasmon shift on the polarization of the impinging light is indeed expected. In case of an exciting p-polarized light, the situation is reversed. Indeed, for small and large α angles ($0°<\alpha<35°$ and $75°<\alpha<90°$), the applied strain yields a blue-shift of the plasmon while, for intermediate angles ($35°<\alpha<75°$), a red-shift is expected. Again, we only consider the interval $60°<\alpha<90°$ for which r decreases upon stretching. In this angular region, the plot of Fig. 11b indicates both a red- and a blue-shift of similar entity that hence compensate each other. Indeed, this conclusion is experimentally verified in Fig. 11d, where the overall plasmonic red-shift is very limited for the sample excited with p-polarized light and the main result is a mere broadening of the plasmon band.

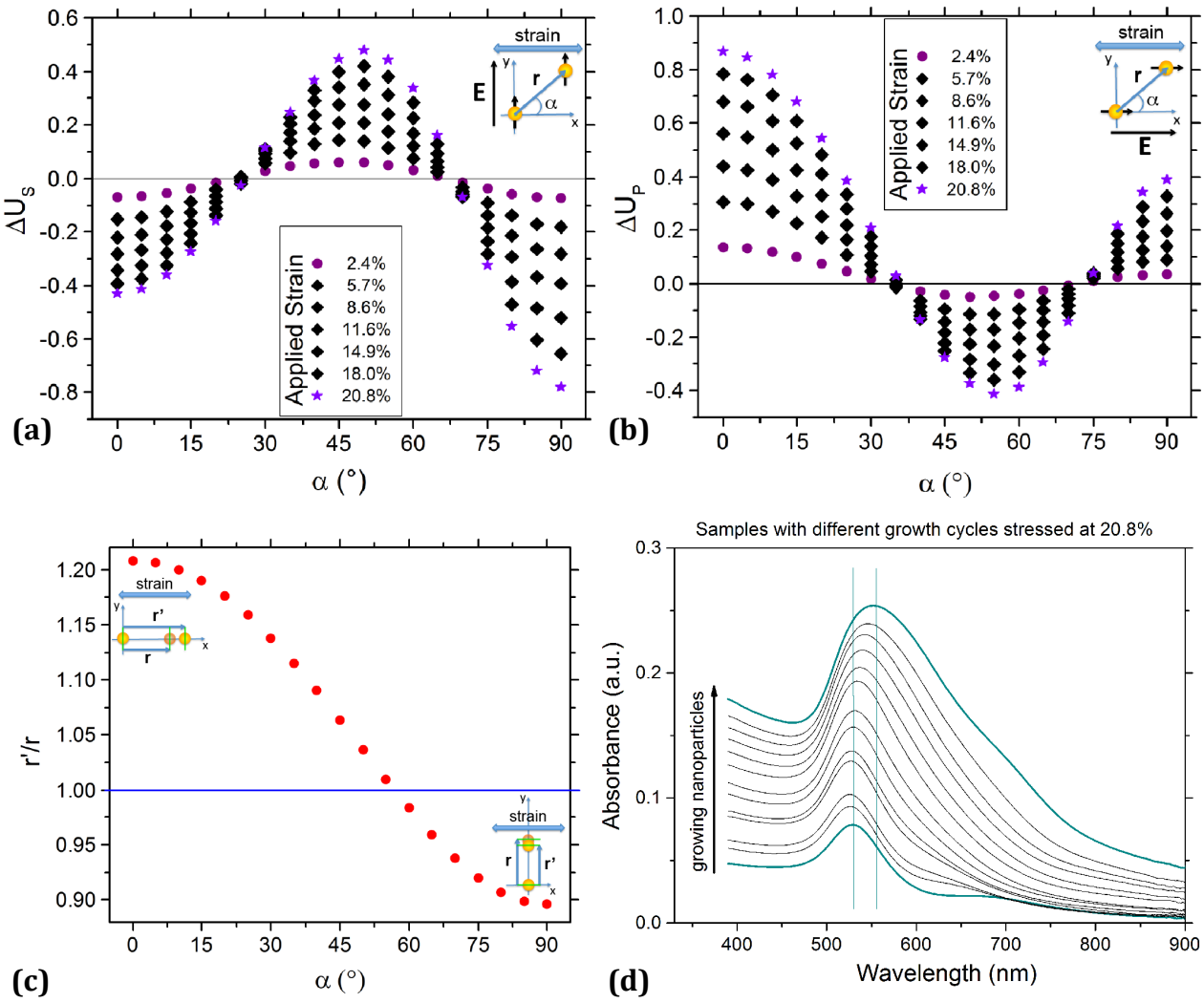

Figure 11. Stretched-unstretched interaction energy variation (relative to the initial value of the interaction energy) plotted as a function of the angle made by the inter-dipole axis with the x-axis both for **(a)** s- and **(b)** p-polarized exciting field. Note that this is true for all initial distances r. **(c)** Plot of the ratio between the inter-particle distance (center-to-center) before (r) and after stretching (r'). The upper left and lower right insets show the condition of two gold nanoparticles that, upon stretching, respectively undergo an increase and a decrease of their inter-particle distance; **(d)** Extinction spectra of the gold nanoparticle coated PDMS samples undergoing different cycles of growth of the particles with an applied strain of 20.8%. Samples have been excited with a p-polarized electric field.

IV.7 Coupling and Plasmon Ruler

Above considerations explain the strong polarization dependent behaviour of the amorphous and initially isotropic samples when stretched by about 20% or even less. Key to this behaviour is the growing of the particle size such that the gap s between them (more precisely s/D) allows weak coupling. Upon stretching, this coupling is weakened in one direction (parallel to the stretching) and enhanced in the perpendicular one. Indeed, a 10% reduction of the initial centre-to-centre distance of the particles (corresponding to 3.9 nm) represents an important 56% change of the particle gap s (reduction from 7 nm to 3.1 nm). In order to better understand how this change of gap can influence the plasmonic behaviour of the system, it is useful to calculate the plasmonic shift normalized to the single-particle resonance wavelength $\Delta\lambda_i / \lambda_0$ as a function of the normalized gap (s/D) existing between nanoparticles. To enable this calculation, a MatLab code exploiting a k-neighbours algorithm has been implemented and exploited for the SEM micrographs of samples with not-grown and grown particles (Fig. 12a,b). The code enables the identification of the particle centers (Fig. 12a) and calculates the distance r between each particle and its nearest neighbours. The detailed procedure utilized to perform the calculations for different growth cycles of the particles is reported in next paragraph. The obtained dependence of $\Delta\lambda_i / \lambda_0$ on s/D (Fig. 12b) is exponential and independent of particle growth and sample stretching state. The solid red curve represents the plasmon ruler equation

$$\frac{\Delta\lambda}{\lambda_0} = k \exp\left(-\frac{s}{\tau D}\right) \qquad (4)$$

with parameters k=0.369±0.038 and τ=0.119±0.010 which are typical for a system made of gold nanospheres. This curve is well in agreement with experimental data and confirms

the plasmonic coupling behaviour of our system. In our knowledge, this is the first time that the plasmon ruler equation has been verified in an amorphous system.

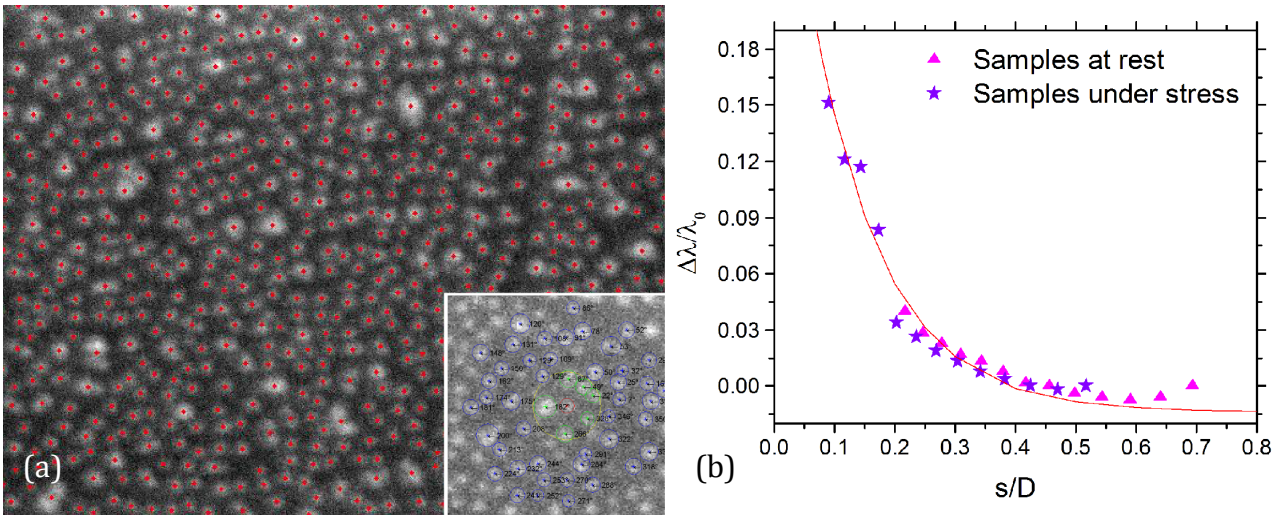

Figure 12. (a) Result of the image analysis performed on the SEM micrograph of Fig. 2a. In red, the centers of particles are depicted as identified by a MatLab code implemented to the scope. In the inset of the figure, the nearest neighbours (circled in green) and all other neighbours (circled in blue) of a single particle are marked; (b) Results of Fig. 3b have been reconsidered by taking into account the average distance between nearest neighbour particles r=39nm and a linear growth of particles from D_0=23nm to D_{12}=32nm. The variable has been calculated as $s/D_i=(r-D_i)/D_i$ for the experiments "at rest" and as $s'/D_i=s(1-f/2)/D_i$ for the experiments "under stress" (f = strain).

IV.7.1 Calculation of $\Delta\lambda_i/\lambda_0$ and s_i/D_i values for extinction experiments performed on samples whose nanoparticles have undergone i growth cycles

The resonance peak wavelength λ_i, measured on the sample whose nanoparticles have undergone a number i of growth cycles (inset of Fig. 9b), was utilized to calculate the plasmonic shift normalized to the single-particle resonance wavelength $\Delta\lambda_i/\lambda_0=(\lambda_i-\lambda_0)/\lambda_0$ Calculated values of $\Delta\lambda_i/\lambda_0$ (with i=0,…,12) have been plotted as a function of s/D for the samples both at rest and under stress.

In order to obtain the average diameter D_i of the nanoparticles grown i times, we assumed a linear growth of the particles from the initial D_0=23nm (nanoparticles not grown) to D_{12}=32nm (obtained after twelve growing steps). The average D_0 and D_{12} values for particle diameters with 0 and 12 growth cycles respectively have been calculated by a MatLab script, which analysed the SEM images of the related samples; in particular, images were binarized and, as a result, coordinates and diameters of separated particles were determined (Fig. 12a). Subsequently, a K nearest neighbours algorithm was applied to calculate distances (and angles between) the closest particles. This analysis yields a nearest neighbour (center-to-center) separation of r=39 nm (arithmetic average). The r values for different stretching states have been calculated by assuming an elastic elongation (and compression in the perpendicular direction) of the sample. From r values at different stretching states and D at different number of growth cycles, s/D values have been calculated as $s_i/D_i=(r-D_i)/D_i$ for the experiments at rest. As for the experiments with samples under stress, results of Fig. 11a and 11c indicate that, during a stretching experiment while illuminating the sample with s-polarized light, a red-shift of the plasmonic resonance wavelength occurs. Responsible of this shift is the plasmonic coupling effect that is preferentially due to dimers with high values of the angle α ($60°<\alpha<90°$) (see Fig. 4c). As such, we can assume:

$$\frac{s_i'}{D_i} = \frac{r' - D_i}{D_i} = \frac{r\left[\left(1+f\right)^2 \cos^2\alpha + \left(1-0.5f\right)^2 \sin^2\alpha\right]^{1/2} - D_i}{D_i} \cong \frac{r\left(1-0.5f\right) - D_i}{D_i} \qquad (5)$$

where f is the applied strain while the factor 0.5 represents the Poisson's coefficient of the PDMS substrate.

IV.8 References

1. Willets, K. A. & Van Duyne, R. P. in *Annual Review of Physical Chemistry* Vol. 58 *Annual Review of Physical Chemistry* 267-297 (2007).

2. Haes, A. J., Zou, S. L., Schatz, G. C. & Van Duyne, R. P. A nanoscale optical biosensor: The long range distance dependence of the localized surface plasmon resonance of noble metal nanoparticles. *Journal of Physical Chemistry B* **108**, 109-116, doi:10.1021/jp0361327 (2004).

3. Li, J. F. *et al.* Shell-isolated nanoparticle-enhanced Raman spectroscopy. *Nature* **464**, 392-395, doi:10.1038/nature08907 (2010).

4. Rockstuhl, C., Lederer, F., Etrich, C., Pertsch, T. & Scharf, T. Design of an artificial three-dimensional composite metamaterial with magnetic resonances in the visible range of the electromagnetic spectrum. *Physical Review Letters* **99**, doi:017401

5. Kinnan, M. K. & Chumanov, G. Plasmon Coupling in Two-Dimensional Arrays of Silver Nanoparticles: II. Effect of the Particle Size and Interparticle Distance. *Journal of Physical Chemistry C* **114**, 7496-7501, doi:10.1021/jp911411x (2010).

6. Cunningham, A., Muhlig, S., Rockstuhl, C. & Burgi, T. Coupling of Plasmon Resonances in Tunable Layered Arrays of Gold Nanoparticles. *Journal of Physical Chemistry C* **115**, 8955-8960, doi:10.1021/jp2011364 (2011).

7. Jain, P. K. & El-Sayed, M. A. Plasmonic coupling in noble metal nanostructures. *Chemical Physics Letters* **487**, 153-164, doi:10.1016/j.cplett.2010.01.062 (2010).

8. Jain, P. K., Huang, W. Y. & El-Sayed, M. A. On the universal scaling behavior of the distance decay of plasmon coupling in metal nanoparticle pairs: A plasmon ruler equation. *Nano Letters* **7**, 2080-2088, doi:10.1021/nl071008a (2007).

9. Sonnichsen, C., Reinhard, B. M., Liphardt, J. & Alivisatos, A. P. A molecular ruler based on plasmon coupling of single gold and silver nanoparticles. *Nature Biotechnology* **23**, 741-745, doi:10.1038/nbt1100 (2005).

10. Brown, K. R., Lyon, L. A., Fox, A. P., Reiss, B. D. & Natan, M. J. Hydroxylamine seeding of colloidal au nanoparticles. 3. Controlled formation of conductive Au films. *Chemistry of Materials* **12**, 314-323, doi:10.1021/cm980066h (2000).

11. Brown, K. R. & Natan, M. J. Hydroxylamine seeding of colloidal Au nanoparticles in solution and on surfaces. *Langmuir* **14**, 726-728, doi:10.1021/la970982u (1998).

12. Brown, K. R., Walter, D. G. & Natan, M. J. Seeding of colloidal Au nanoparticle solutions. 2. Improved control of particle size and shape. *Chemistry of Materials* **12**, 306-313, doi:10.1021/cm980065p (2000).

13. Enders, D., Nagao, T., Pucci, A., Nakayama, T. & Aono, M. Surface-enhanced ATR-IR spectroscopy with interface-grown plasmonic gold-island films near the percolation threshold. *Physical Chemistry Chemical Physics* **13**, 4935-4941, doi:10.1039/c0cp01450h (2011).

14. J. Liu and Yi Lu, J.AM CHEM SOC. 2004, 126, 12298-12305

15. C.D. Keating, M.D. Musick, M.H. Keefe, and M.J. Natan, JChemED.chem.wisc.edu, Vol. 76, No.7, July 1999

16. M.K. Kinnan and G. Chumanov, *J. Phys. Chem*. C **2010**, 114, 7496-7501

V Discussion and Conclusions

The main aim of this thesis work has been to study of active plasmonics triggered and driven by external and controlled perturbations as electrical fields, temperature changes and mechanical strains. For this goal two research lines have been developed whose results are discussed in the following section. In both lines, active plasmonic structures have been obtained by bottom-up and self-assembling procedures.

In the first one, the tunable plasmonic device is made of a Policryps grating structure in which a chiral organization of gold nanoparticles is achieved through the presence of a cholesteric liquid crystal. The optical characterization reveals a blue-shift of the plasmonic resonance wavelength due to the application of an external electric field. In case the temperature is changed, a red-shift of the resonance is observed. The two shifts are nearly connected to the change of refractive index of the cholesteric liquid crystal that, in this way, acquires a double function in organizing nanoparticles and tuning their plasmonic properties. Noteworthy, the Policryps template structure shows its versatility as a platform where it is possible to organize a chiral arrangement of gold particles. The merging between top-down and self-assembling procedures to obtain the Policryps structures, and bottom-up and self-assembling techniques in the organization of nanostructures by the soft-matter (cholesteric liquid crystal) is fundamental for obtaining the active plasmonics device.

In the second line of research, the realization of a large area sample is based on bottom-up and self-assembling procedures. Nano-chemistry growth processes are utilized to increase the size of nanoparticles, previously anchored above the elastomeric surface. The obtained optical pad is used to study the coupling between plasmonic dipolar near-fields through externally applied mechanical strains. During experiments, a red-shift and a

change of shape of the plasmonic resonance are observed that are not related to the size of nanoparticles but only to the modification of their reciprocal gap (edge-to-edge distance). This gap is decreased by increasing the sizes of particles and by applying a compression to the elastic substrate. The results of these observations are instead due to coupling processes and can be well identified in the paradigm of the plasmon ruler equation. In our knowledge, this is the first time that this equation has been confirmed with an isotropic and disordered system. Indeed, the influence of the mechanical strength in the coupling processes is evident from the drastic change of the slope of the measured curve: a 10.4% compression, applied perpendicularly to the direction of stretching, corresponds to a decrease of 56% of the reciprocal gap between nanoparticles. In this way, it emerges that a macroscopical mechanical perturbation can deeply change the features of the system at the nanoscale.

With this kind of arrangement of nanoparticles, the unidirectional mechanical strain produces anisotropy in the behaviour of the system when this is observed with polarized light, respectively along and perpendicularly to the longitudinal stretching. If an ordered array of nanostructures is considered, the strong coupling is only related to the direction parallel to the wave field. In our system, at the same time, many dimers participate to the coupling but not all of them in the same way. Indeed, responsible of the coupling will be only those localized in a well-defined double conical region around the single nanoparticle, that has its main axis orthogonal to the direction of stretching and parallel to the polarization of the impinging electrical field.

Another characteristic of this elastic coupling is the reversibility of the process shown by the disappearing of the red-shifted plasmon resonance peak, and the restoring of the initial dipolar plasmonic response. For this reason we exclude phenomena of clusterization or agglomeration in the sample during the stretching.

Finally, a further proof of coupling induced between gold nanoparticles by mechanical strain applied to the structure is well testified by the macroscopic change of colour of sample.

VII Outlook

During this Ph.D path, several ways have been explored to develop innovative and relatively easy technics to realize tunable plasmonic devices.

Future developments regarding Polycryps infiltrated with cholesteric liquid crystal and nanoparticles concern the applicability of this device mainly as a sensor of temperature variations. In fact, as we showed in III.5.2, the increase of temperature of the system produces as a response a 50nm red-shift of the plasmon resonance. This application can be utilized both as a delocalized and localized plasmonic sensor of temperature. The former, to register changes of temperature from an external system; the latter to check a nanoscale variation of temperature of a plasmon-photonics device. This last application is based on the local increase of temperature that takes place around the nanostructure produced by the plasmonic resonance. Because the medium around the particle is, in this case, a thermotropic liquid crystal, this thermal changes, increases the local temperature of the cholesteric with a localized decrease of refractive index of the same. This dielectric modification gives a contemporaneous blue-shift of the diffractive band of the structure (pink curve of figure 2a in III.5.1). A first implementation of the plasmon-photonics thermometer can be as a gauge curve where the peaks of the diffractive band are function of temperature. As such, the device will work as an all-optical device with the synergy of active plasmonics solicitation (resonance red-shift), and relative photonic effect (blue-shift of diffractive band) both checked only by changing the polarization of the spectrometer beam probe.

Regarding the future developments of the elastic pad, for its great versatility and reproducibility, this device can be utilized to realize new and innovative sensor SERS and metamaterial applications.

But to proceed in this direction, a complete characterization needs to be performed. A full control of the growth processes of gold nanoparticles is necessary. A possibility is to obtain gauge curves of nanoparticle size versus number of growth cycles. Moreover, the kinetics of these nano-chemistry processes needs to be investigated.

Parallel to these ones, a complete morphological analysis, by SEM, AFM SNOM, under mechanical strain needs to be performed to check both the structural modification of the sample surface and to acquire the measures of the gap existing between nanoparticles with the sample at rest and during stretching.

The optical characterization, by increasing stretching and particles growth, needs to be continued to check which is the lower threshold before quantum coupling begins and, at the same time, which are the aggregation or clusterization thresholds. This whole investigation must be realized while keeping the PDMS template in elastic conditions.

In the theoretical analysis of experiment results, we need to describe the coupling not only considering a dimer approximation but also with trimer and quadrimer because the distribution of nanoparticles above the sample surface is random and disordered. In parallel with this approach, the near-fields interaction has to be explored by quadrupole coupling approximation.

Once the monolayer characterizations are completed, it is possible to proceed with the realizing of a bilayer. In fact, polyelectrolyte or silane compounds can be utilized to space apart the two layers of grown nanoparticles. At this point, by performing a stretching characterization we will be able to study not only the coupling of planar near-fields but also the volume one.

The aim of this characterization is to improve the properties of these systems and to discover new ones. The full controllability and reversibility of the coupling process by applying a mechanical strain must be considered as a fundamental property of the system.

We conclude this work of thesis asserting that the results obtained by experiments and theoretical analysis, is the first step toward the realization of new devices both sensor and metamaterial applications, and in the improving of all spectroscopical technics that need the strengthening of local fields.

VII Acknowledgements

In this last section I want to express my gratitude to all people with which I collaborated and from whom I have been supported in this three years. I begin in Italian language and then continue in English.

Alla fine di questo lavoro di tesi, che porta a compimento il mio dottorato, sento l'obbligo e nello stesso tempo il piacere di ringraziare tutte quelle persone con cui sia a livello professionale che umano ho potuto interagire. La mia gratitudine, in primis, va al Prof. Cesare Umeton che accogliendomi nel suo gruppo e affidandomi al Prof. Roberto Caputo, mi ha permesso di intraprendere e portare a termine questa esperienza formativa e professionale. Quindi, come già accennato, voglio ringraziare il mio supervisore Prof. Roberto Caputo, con cui è nata anche una bella amicizia, sia per avermi introdotto allo studio della plasmonica su substrati elastomerici e sia per essersi speso molto per l'organizzazione del mio soggiorno all'estero che ha costituito il momento più importante di questo periodo triennale. Inoltre gli sono grato per i consigli che mi ha dato a livello professionale e infine per la grande pazienza dimostrata in questi ultimi periodi di correzzione della tesi. Ringrazio, poi, il dott. Luciano De Sio, amico e collega, con il quale ho iniziato la mia attività sperimentale e in cui ho trovato sempre la disponibilità al confronto. Utilissimi sono stati a tal riguardo i suoi consigli professionali. Ringrazio inoltre la dottoressa Luigia Pezzi per i suoi validi suggerimenti professionali e per la sua amicizia. Inoltre voglio ricordare il tesista ed amico Fabio Cerminara con il quale abbiamo acquisito alcune misure utilizzate poi da lui nella sua tesi di laurea di cui sono stato il correllatore. Infine, ringrazio tutti dottorandi del gruppo che hanno iniziato da poco il loro cammino: Giovanna Palermo, Vincenzo Caligiuri e Domenico Alj.

Passo ora ai saluti in inglese per tutti coloro che ho incontrato e con cui ho collaborato nel mio periodo Ginevrino.

I want to thank Prof. Dr. Thomas Bürgi, which permitted my internship in his group in the physical-chemistry department of the University of Geneva. In this year, with his professional and human support, I worked very well and in his group I found a good human and professional enviroment with people that have been not only collegues but have been became also good friends.

With Prof. Bürgi, I want to thank the others members of jury: Prof. Prof. Paolo Mariani from the department of Scienze della Vita e dell'Ambiente, Università Politecnica delle

Marche, Prof. Gino Mariotto from the department of Informatica, Università di Verona, Dott. Angelico Ruggero PhD University of Molise, for taking the time to read this thesis and be present for the examination.

In the Burgi group, firstly I want to thank Dott. Alastair Cunningham. He was the first people from this group, with which I collaborated in Nanogold project during the second year of my Phd and during the last months of his Phd , in Geneva. Then, I want to thank Doct. Mahshid Checkini for her collaboration and with which I had many opportunities of professional comparison. Continuing, my gratitude goes to Doct. Gérard Klein for his disponibility to supervise my chemical work. Then I want to thank Doct. Igor Dolamic, Doct. Noelia Barrabes Rabanal, Doct. Patric Oulevy, Dr. Stefan Knoppe, Doct. Ahmed Bouhekka, Doct. Harekrishna Gosh, Doct. Birte Varnholt for their collaboration and friendship and then my gratitude go to Doct. Raymond Azoulay and to Isabel Garin for their great disponibility.

Quindi voglio fare uno speciale ringraziamento al Prof Raffaele Agostino, mio relatore di tesi e amico carissimo che ha incoraggiato questo mio percorso di dottorato.

Alla fine, voglio fare un grande ringraziamento alla mia famiglia. In primis mia madre e mia sorella che mi hanno sostenuto e incoraggiato durante questi tre anni e in special modo durante l'anno passato a Ginevra. Senza la loro forza, la forte presenza e il grande incoraggiamento e il loro amore, sarebbe stato molto difficile affrontare le varie sfide che si sono presentate. Poi la mia gratitudine va a mio fratello e mia cognata, con i quali, durante il periodo trascorso in Svizzera, ho trascorso quei pochi fine settimana italiani a Pinerolo. Quindi voglio ringraziare i miei zii e miei cugini per la loro costante vicinanza. Inoltre un ringraziamento va ai miei amici italiani di Crotone, Cosenza e Ginevra con i quali ho passato bei momenti di convivialità. In fine ringrazio la mia collega, la dottoressa Caterina Maria Tone per la pazienza e l'amicizia dimostratami in questo ultimo periodo.

Infine il mio ringraziamento va a Colui che ha guidato I miei passi e ha posto sul mio cammino queste persone.